High-spin states in ^{157,158}Er and ^{158,159}Tm

R. Holzmann, M. Loiselet, M. A. Van Hove, and J. Vervier
Institut de Physique Nucléaire, B-1348 Louvain-la-Neuve, Belgium
(Received 14 May 1984)

High-spin states in ^{157,158}Er and ^{158,159}Tm have been studied via the ^{122}Sn(^{40}Ar,5,4n) and ^{141}Pr(^{22}Ne,5,4n) reactions, respectively, using in-beam gamma-ray spectroscopy techniques which included γ-γ coincidence, angular correlation, angular distribution, excitation function, and multiplicity measurements. The favored ($\pi=+$, $\alpha=+\frac{1}{2}$) $i_{13/2}$ neutron band in ^{157}Er has been established up to the $\frac{53}{2}^+$ level ($\hbar\omega=0.417$ MeV), and the favored ($\pi=-$, $\alpha=-\frac{1}{2}$) and unfavored ($\pi=-$, $\alpha=+\frac{1}{2}$) $h_{11/2}$ proton bands in ^{159}Tm, up to the $\frac{59}{2}^-$ ($\hbar\omega=0.454$ MeV) and $\frac{61}{2}^-$ ($\hbar\omega=0.480$ MeV) levels, respectively, i.e., well above the range of rotational frequency $\hbar\omega$ where a second backbending has been observed in the neighboring even-even nuclei. In ^{158}Er, the yrast levels have been observed up to 38^+, and in ^{158}Tm, up to 25^-. The favored $i_{13/2}$ band of the odd-N nucleus ^{157}Er displays a strong upbending at $\hbar\omega=0.40$ MeV, whereas, in the two branches of the $h_{11/2}$ yrast band of the odd-Z nucleus ^{159}Tm, no alignment effect has been observed between $\hbar\omega=0.27$ and 0.48 MeV. The experimental results have been analyzed in the framework of the cranked shell model. On the basis of blocking arguments and cranked shell model calculations, the obtained results show that the second backbending in the yrast band of even-even nuclei near $A=158$ is due to an $h_{11/2}$ proton alignment. The signature splitting of the intrinsic excitation energies (Routhians) and aligned angular momenta in ^{159}Tm has been reproduced in cranked shell model calculations by introducing a triaxial deformation. The observed steep rise of the $B(M1)/Q_0^2$ values in the favored and unfavored bands of ^{159}Tm are consistent with an increase of $|g_K-g_R|$ at the first backbending due to the alignment of a neutron pair around $\hbar\omega=0.27$ MeV. The evolution of the kinematical and dynamical moments of inertia at very high rotational frequencies ($\hbar\omega>0.50$ MeV) yields information on the nuclear pairing correlations in this frequency range.

I. INTRODUCTION

With the advent of high-energy heavy-ion beams and improved γ-ray detection techniques, it has become possible to study excited states in collectively rotating nuclei up to very high spins. One of the most striking features that showed up in these investigations is the so-called second backbending. Since its discovery[1] in the yrast band of ^{158}Er around spin 28, it has also been observed[2-5] in several other even-even nuclei near $N=90$, i.e., ^{160}Yb, ^{156}Er, and ^{162}Hf.

It was first suggested by Faessler and Ploszajczak[6] that the second backbending in these nuclei is due to the rotation alignment (RAL) of a pair of $h_{11/2}$ protons along the axis of collective rotation. Indeed, the first backbending observed in many deformed even-even nuclei of the rare-earth region[7] has been shown to arise from the RAL of a pair of $i_{13/2}$ neutrons. This explanation, first put forward by Stephens and Simon,[8] has later been confirmed experimentally by Grosse, Stephens, and Diamond[9,10] who interpreted data on the yrast bands of the odd-neutron nuclei ^{157,159}Er and of the odd-proton nuclei ^{157,159,161}Ho on the basis of blocking arguments. Although several theoretical works, among which cranking Hartree-Fock-Bogoliubov (CHFB) calculations[11] and cranked shell model (CSM) calculations,[12] strongly suggest the $h_{11/2}$ proton nature of the second backbending observed in the above-mentioned mass region, some authors claim that this phenomenon could be due to the RAL of an $h_{9/2}$ neutron pair, at least in ^{156}Er.[4,13] There has been so far no experimental evidence that could help in solving this controversy by identifying unambiguously the nucleon pair involved in the second backbending near $N=90$.

In the present work, we report on an experimental investigation of the yrast bands in the odd-neutron nucleus $^{157}_{68}$Er$_{89}$ and in the odd-proton nucleus $^{159}_{69}$Tm$_{90}$, up to the range of rotational frequencies where the second backbending has been seen in the neighboring even-even nuclei ($\hbar\omega\cong0.40$ MeV). These two odd-mass nuclei were selected because both of them lie between even-even nuclei that are known to display a second backbending, i.e., ^{156}Er and ^{158}Er for ^{157}Er, and ^{158}Er and ^{160}Yb for ^{159}Tm. Both nuclei have been studied previously at low and medium spins: the favored band in ^{157}Er has been investigated up to the level with $I^\pi=\frac{41}{2}^+$,[9,14] and the favored and unfavored bands in ^{159}Tm up to the levels with $I^\pi=\frac{47}{2}^-$ and $\frac{49}{2}^-$, respectively.[15] In our work, we have extended these bands by in-beam γ-ray spectroscopy up to $\frac{53}{2}^+$ in ^{157}Er, and $\frac{59}{2}^-$ and $\frac{61}{2}^-$ in ^{159}Tm, corresponding to rotational frequencies well above the critical value for the second backbending.

We have interpreted our data in the framework of the CSM (Refs. 12 and 16) with special emphasis on the blocking effect. We have definitely confirmed the proton origin of the second backbending in the nuclei near

$N=90$. Furthermore, our data give strong evidence for a triaxial shape in the nucleus ^{159}Tm and for a change of its magnetic properties at the first backbending, as well as information on the nuclear pairing correlations above $\hbar\omega=0.50$ MeV in the nuclei near $A=158$. Finally, we have also obtained in our experiments information on high spin states in the even-even nucleus ^{158}Er and in the odd-odd nucleus ^{158}Tm.

Preliminary results from the present work have already been published elsewhere.[17,18] Recently, similar and independent measurements have been presented on the nucleus ^{159}Tm by Riedinger *et al.*,[19] and on the nucleus ^{157}Er by Riley *et al.*[20]. The results of these authors will be compared to our experimental data.

II. EXPERIMENTAL TECHNIQUES AND DATA REDUCTION

Excited states in ^{157}Er were populated by the ^{122}Sn(^{40}Ar,5n)^{157}Er reaction, with ^{40}Ar beams of various energies between 160 and 200 MeV. A stack of five self-supporting metallic tin foils of 400 μg/cm^2, enriched to 95% in ^{122}Sn and separated by 0.6 mm spacers, was used as the target in all experiments involving the nucleus ^{157}Er. This particular arrangement allowed us to study the γ decay of the nuclei in flight, thus avoiding the line broadening due to the Doppler shift attenuation (DSA) effect in thick materials, which is important for the very short-lived ($\lesssim 1$ ps) high-spin states. For the nucleus ^{157}Er, γ-γ coincidences, γ-ray multiplicities, and relative excitation functions were measured yielding transition energies, relative intensities, and multipolarities. In these experiments, information on the nucleus ^{158}Er, arising from the $4n$ reaction channel, was also obtained as a by-product.

The energy levels of ^{159}Tm were studied by the ^{141}Pr(^{22}Ne,4n)^{159}Tm reaction, with ^{22}Ne beams of 110 and 120 MeV. Here, a stack of four self-supporting equally spaced (0.6 mm) metallic praseodymium foils of 1.3 mg/cm^2 was used as a target. Because of the high chemical reactivity of this metal, the foils were coated on both sides by a thin (≈ 15 μg/cm^2) nickel layer. For the nucleus ^{159}Tm, γ-γ coincidences were measured, as well as angular distributions with a thick (36 mg/cm^2) praseodymium target. In these experiments, data on the odd-odd nucleus ^{158}Tm were also obtained via the 5n reaction channel.

All measurements were carried out at the Cyclone accelerator facility of Louvain-la-Neuve, using the newly developed electron-cyclotron resonance (ECR) continuous-current heavy-ion source ECREVIS.[21]

A. The γ-γ coincidence measurements

1. Experimental setup

The experimental setup used in the γ-γ coincidence measurements is shown in Fig. 1. It included (a) four 60 cm^3 Ge(Li) detectors with an efficiency of about 12%, with respect to a 7.6×7.6 cm NaI(Tl) scintillator and a resolution of 2.2 keV at 1.33 MeV, placed at angles of 0°, 90°, 150°, and −150° with respect to the beam axis; and (b)

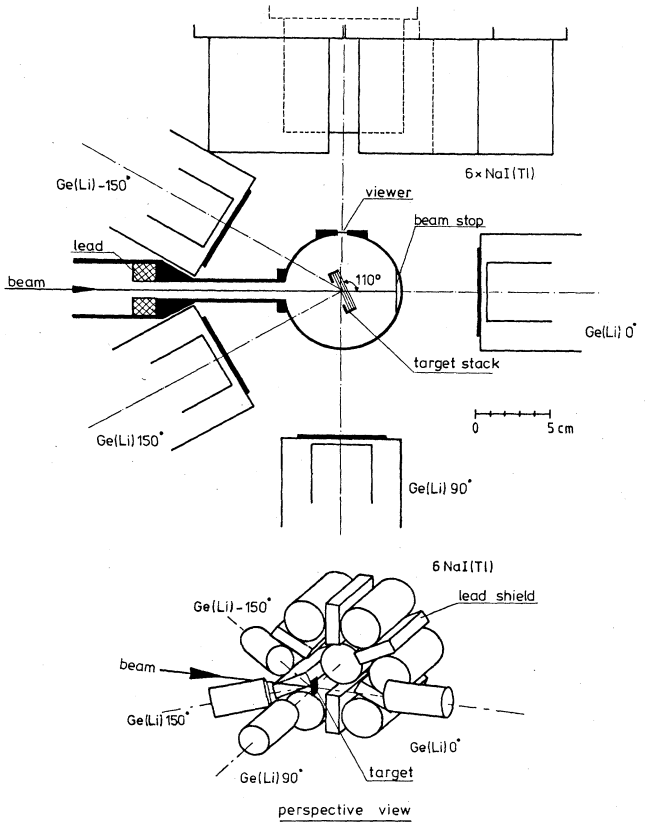

FIG. 1. Experimental setup used in the γ-γ coincidence measurements described in Sec. II A *1*.

a multiplicity filter, consisting of six 7.6×7.6 cm NaI(Tl) detectors whose axis was at −90°. The residual heavy ion beam was stopped 40 mm behind the target, in a thick (127 μm) natural lead foil. The various detectors were shielded against the x-ray flux produced by the beam impact on this stopper foil by absorbers consisting of 0.1 mm Ta, 0.6 mm Cd, and 0.5 mm Cu foils for the Ge(Li) detectors, and of a 1 mm Cu foil for the NaI(Tl) detectors.

In the coincidence experiments, two out of the four Ge(Li) detectors were required to fire in coincidence with each other, and with at least one out of the six NaI(Tl) counters, as well as with a cyclotron beam burst. Using standard fast-slow electronics, four-parameter events, including the energies observed in the two Ge detectors that fired, the number of firing NaI(Tl) counters (fold), and the timing information ($\Delta t_{\gamma 1\text{-}\gamma 2}$), were written onto magnetic tape for off-line analysis. During the experiments, singles and some coincidence spectra were accumulated in the computer for monitoring purposes. For each run, roughly 200×10^6 events were recorded in this way.

The amplifier gains of the four Ge(Li) detectors were approximately matched taking into account the angle-dependent Doppler shifts. The detectors were energy and efficiency calibrated using standard (^{133}Ba and ^{152}Eu) γ-ray sources.

2. *Analysis of the coincidence data*

In the off-line analysis of the coincidence data, the four-parameter events ($E_{\gamma 1}$, $E_{\gamma 2}$, fold, $\Delta t_{\gamma 1\text{-}\gamma 2}$) were sorted into $E_{\gamma 1} \times E_{\gamma 2}$ matrices of 2048×2048 channels, with a dispersion of about 0.75 keV/channel. During the processing, the approximately matched energy scales of the Ge(Li) detectors were precisely readjusted to a common scale, in order to preserve the original energy resolution. The resulting coincidence matrices were furthermore corrected for random coincidences, and finally symmetrized, to enhance the statistics and to simplify the later analysis.

In a typical γ-γ coincidence experiment with bare Ge(Li) detectors, only about 2% of the recorded events are photopeak-photopeak events; the rest, i.e., about 98%, involve Compton scattering in at least one of the two detectors. This means that meaningful structures may be hidden in a continuum of mostly "uncorrelated" events. A numerical method has been proposed by Andersen *et al.*,[22] which allows the almost complete removal of the Compton events from the coincidence matrix. This method is based on the assumption that the probability of obtaining an event at energies (E_i, E_j) in the two-dimensional plane of coincidences is given in first order by $(\sum_k N_{ik} \sum_l N_{lj})/(\sum_{kl} N_{lk})^2$, where N_{ij} represents the number of events in the channel (i,j) of the matrix. The number of non-photopeak-photopeak events in this channel $(\tilde{N}_{ij})$ can therefore be estimated by calculating the product of this probability by the total content of the matrix, i.e., $\sum_{kl} N_{lk}$. Again in first order, the number of photopeak-photopeak coincidences is then given by $\Delta N_{ij} = N_{ij} - \tilde{N}_{ij}$. A better estimate of this number can be obtained by subtracting the absolute value of the first order result (ΔN_{ij}) from the raw matrix (N_{ij}) before calculating $\tilde{N}_{ij}$. Applying this method repeatedly leads to an iterative procedure in which the step $n \rightarrow n+1$ reads

$$\Delta N_{ij}^{(n+1)} = N_{ij} - \frac{\sum_k (N_{ik} - |\Delta N_{ik}^{(n)}|) \sum_l (N_{lj} - |\Delta N_{lj}^{(n)}|)}{\sum_{kl} (N_{lk} - |\Delta N_{lk}^{(n)}|)} .$$

This improved method, which was first proposed by Herskind,[23] can be applied until consecutive steps show no significant deviations anymore.

The uncorrelated continuum was subtracted iteratively from all the coincidence matrices accumulated in this work before setting gates on discrete transitions. Convergence was usually reached after about 50 iterative steps. From the corrected matrices, spectra coincident with discrete transitions were constructed by projecting an appropriate number of rows (or columns) onto the corresponding axis, and by subtracting a spectrum resulting from a gate placed on the residual continuum near these transitions. Although subtracting the uncorrelated continuum prior to placing the gates does not reduce the statistical errors, we have found that it simplified the analysis and lowered the systematic errors due to possibly inadequate choices of the background gates. Figure 2 shows an example of the improvement one can obtain by this method.

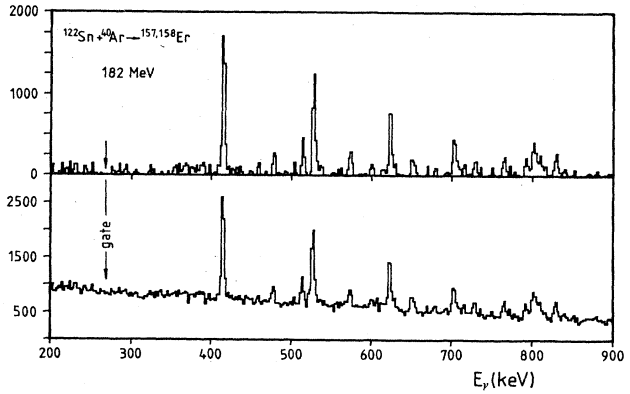

FIG. 2. Comparison between the coincidence spectra before (lower) and after (upper) the application of the background-substraction method described in Sec. II A 2. The gate is set on the 266.36 keV, $\frac{17}{2}^+ \rightarrow \frac{13}{2}^+$ transition in ^{157}Er, and the procedure has been iterated 50 times.

The γ-γ coincidence measurements also yielded information on the multipole character of the observed transitions by the fact that the four Ge(Li) detectors were placed at angles which allowed analyzing of the angular correlation effects. Indeed, the different coincidence pairs that were recorded corresponded to the following pairs of angles: 0°-30°, 30°-30°, and 30°-90°, + 150° and −150° being equivalent to 30°. Although a formalism of multiple angular correlations has been developed,[24] it is much too cumbersome to be of easy practical use in the present case. Fortunately, in the case of stretched γ-ray cascades between high-spin ($I \geq 20\hbar$) states, a semiclassical approximate formalism can be used to estimate the correlation functions with sufficient accuracy.[24,25] Along this way, the intensity ratios $I_\gamma(0°)/I_\gamma(90°)$ and $I_\gamma(30°)/I_\gamma(90°)$ were computed for the different possible multipolarities ($L=1$, $\Delta I=0,1$ and $L=2$, $\Delta I=0,1,2$), under the assumption that the multiplicity filter triggered on a cascade consisting, on the average, of 80% stretched quadrupole transitions and 20% stretched dipole transitions. These values are characteristic for deformed nuclei in the rare-earth region.[26] By comparing the measured intensity ratios to the calculated ones, the multipole character of the detected γ rays could be determined in most cases.

Finally, after having been smoothed and squeezed to a size of 256×256 channels, the continuum-subtracted coincidence matrices served to investigate the γ_1-γ_2 energy correlation patterns in the $E_{\gamma 1} \times E_{\gamma 2}$ plane, especially the width of the central valley which is known to be related to the collective moment of inertia of the nucleus.[22,27,28]

B. Other measurements

1. *Multiplicities and excitation functions*

For the ^{122}Sn + ^{40}Ar reaction, average γ-ray multiplicities $\langle M_\gamma \rangle$ were measured at beam energies of 160, 180, and 190 MeV, as well as relative excitation functions at beam energies of 160, 170, 175, 180, 185, 190, and 200 MeV. The experimental setup used for these experiments

is shown in Fig. 3. The location at backward angles of the multiplicity filter, consisting of six 7.6×7.6 cm NaI(Tl) detectors, was chosen in order to reduce angular correlation effects on the derived multiplicities as much as was feasible. Calibrated γ-ray sources were used to determine the absolute detection efficiencies of the NaI(Tl) counters. They were found to be constant within 10% between 200 keV and 2 MeV; the mean value used in the analysis of the multiplicity data was $\bar{\Omega}_\gamma = 0.0186(9)$. The neutron detection efficiency of the NaI(Tl) counters was measured with a ^{252}Cf spontaneous fission source ($\bar{E}_n = 2.14$ MeV), yielding a ratio $\bar{\Omega}_n/\bar{\Omega}_\gamma = 0.30(4)$.

With the multiplicity setup, prompt coincidence events (E_γ, fold, $\Delta t_{\text{Ge(Li)-beam}}$) were recorded, and p-fold ($p = 0, 1, \ldots, 6$) spectra were constructed on line for the various beam energies. The multiplicity data were analyzed with the nonlinear reduction method proposed by Ockels,[29] including corrections for the detection of evaporated neutrons[30] and for the subsisting angular correlation effects.[25] The first correction reduced the multiplicity on the average by about 7%, and the second correction by about 5%.

For the excitation function measurements, single Ge(Li) spectra were recorded at 0°, requiring a prompt coincidence ($\Delta t \leq 15$ ns) with the cyclotron beam burst in order to reduce the contribution from long-lived activities. The extracted transition yields were then normalized to the Pb $K\alpha$ and $K\beta$ x-ray yields from the thick lead stopper foil.

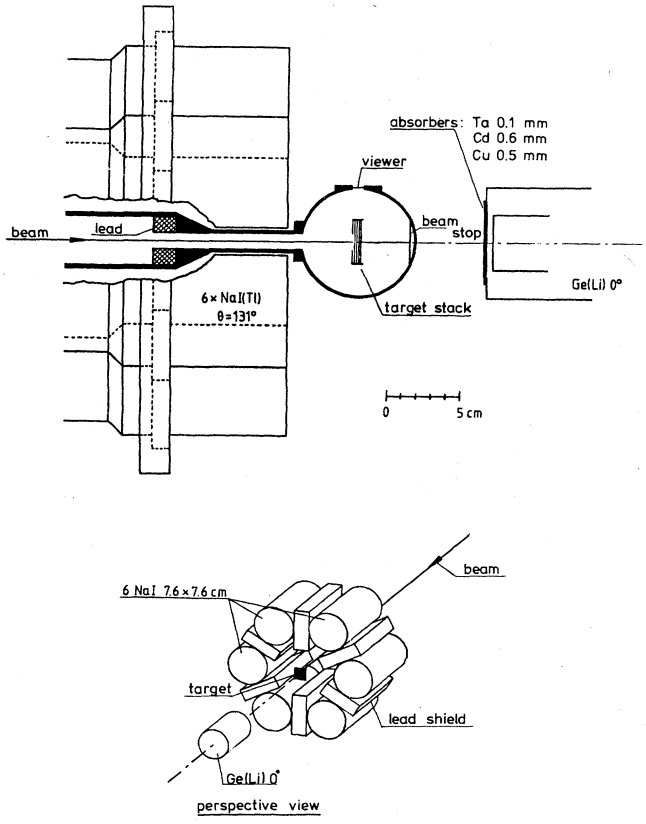

FIG. 3. Experimental setup used in the measurements of the multiplicities and excitation functions described in Sec. II B *1*.

2. *Angular distributions*

For the ^{141}Pr + ^{22}Ne reaction, angular distributions were measured at a beam energy of 110 MeV with a thick (35 mg/cm^2) praseodymium target. For this purpose, singles spectra were recorded with three Ge(Li) detectors placed at 0°, 30°, and 90°, 12 cm from the target. Some spectra were also recorded with calibrated γ-ray sources placed near the target in order to get a very precise energy calibration for the three detectors. From these measurements, accurate transition energies, branching ratios, and multipole mixing ratios were deduced for the nucleus ^{159}Tm. The resulting angular distributions yielded the usual A_2 and A_4 coefficients of a Legendre polynomial expansion.

III. EXPERIMENTAL RESULTS

A. The nucleus ^{157}Er

The total $\geq$ onefold coincidence spectrum, obtained with the multicounter setup described in Sec. II A for the ^{122}Sn + ^{40}Ar reaction at a beam energy of 182 MeV, is shown in Fig. 4. At this bombarding energy, the yields of the various reaction channels were $\cong$20% for ^{156}Er, $\cong$48% for ^{157}Er, $\cong$30% for ^{158}Er, and $\cong$2% for ^{159}Er. As already mentioned, γ-γ coincidences, γ-ray multiplicities, and relative excitation functions were measured for the nucleus ^{157}Er. In the analysis of the coincidence experiment, gates were set on all transitions known in this nucleus from previous works,[9,14] as well as on the new transitions in this nucleus observed in the present work. Some of the projected spectra are represented in Figs. 5(a)—(c).

The detailed analysis of the complex multiplet present

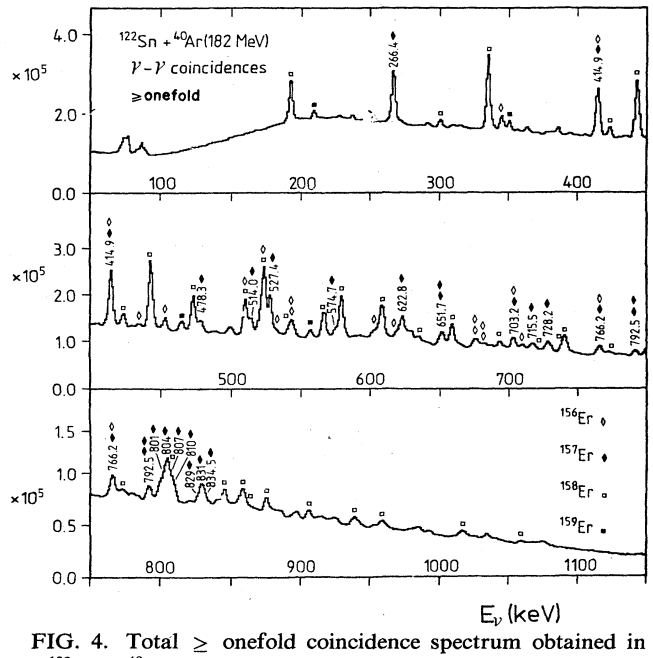

FIG. 4. Total $\geq$ onefold coincidence spectrum obtained in the ^{122}Sn + ^{40}Ar(182 MeV) reaction. The transitions belonging to ^{157}Er and ^{158}Er are also listed in Tables I and II, respectively.

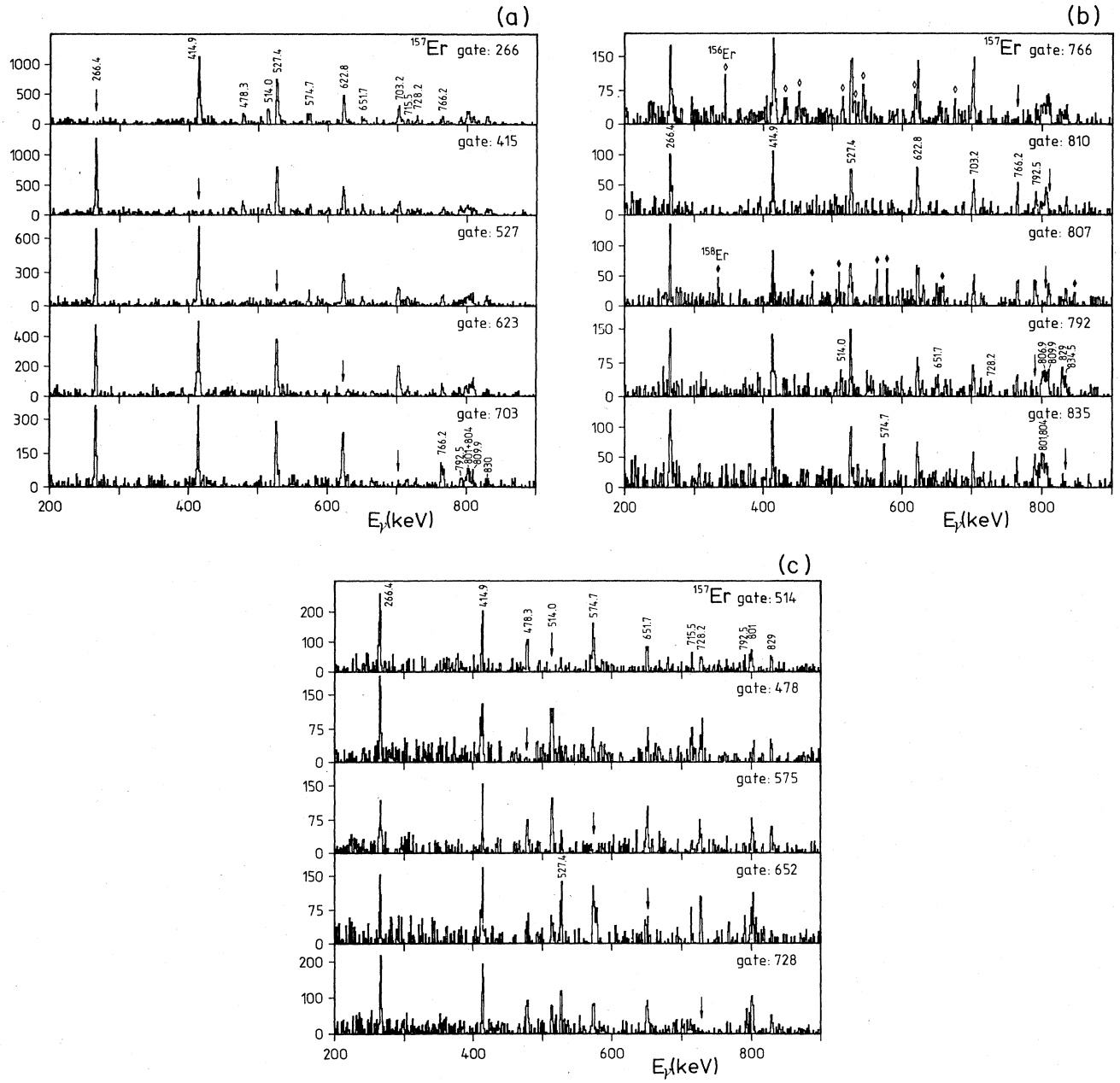

FIG. 5. Coincidence projections obtained with the ^{122}Sn(^{40}Ar,5n)^{157}Er reaction at $E(^{40}\text{Ar}) = 182$ MeV. The gates are marked by arrows on each spectrum. Transitions belonging to ^{156}Er and ^{158}Er are indicated by open and solid diamonds, respectively. The other transitions belong to ^{157}Er and are also listed in Table I.

around 800 keV (Fig. 6) reveals that it contains at least four γ-rays belonging to the nucleus ^{157}Er, at 801.3, 804.1, 806.9, and 809.9 keV, in addition to the 805.7 keV line which is known[1,32] to belong to ^{158}Er. The different projections of Fig. 5 show that the 809.9, 806.9, 792.5, and 834.5 keV transitions extend the favored band in ^{157}Er up to higher spins, i.e., deexcite the levels with $J^\pi = \frac{41}{2}^+$, $\frac{45}{2}^+$, $\frac{49}{2}^+$, and $\frac{53}{2}^+$, respectively. The 478.3, 514.0, 574.7, 651.7, 728.2, 801.3, 829.0, 804.1, and 792.5 keV transitions belong to a weakly populated sideband in ^{157}Er. The measured intensity ratios $I_\gamma(0°)/I_\gamma(90°)$ and $I_\gamma(30°)/I_\gamma(90°)$ are consistent with stretched $E2$ transitions in all cases, except maybe for the 514.0 transition which is contaminated by the 511 keV annihilation radiation. The proposed assignments of the newly observed transitions are confirmed by the multiplicity and excitation function data. The order of the transitions is mainly based on relative intensities determined from coincidence and singles spectra. All results on the nucleus ^{157}Er are summarized in Table I.

The partial level scheme of ^{157}Er constructed from our data is shown in Fig. 7. The connection between the sideband and the favored band could not be completely elucidated, although the 715.5 keV transition seems to play a

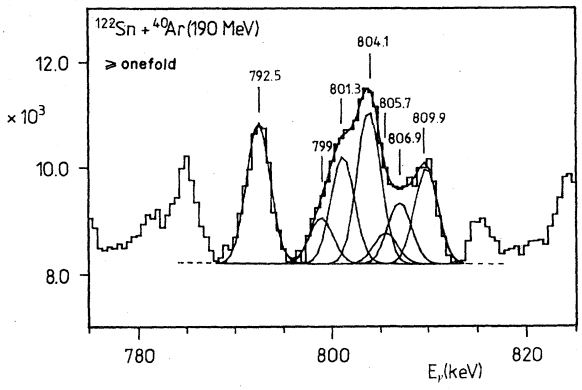

FIG. 6. Detailed analysis of the complex multiplet around 800 keV in the total ≥ onefold coincidence spectrum obtained with the ^{122}Sn + ^{40}Ar(182 MeV) reaction. The transitions belong to ^{157}Er and ^{158}Er (Tables I and II), except for the weak 799 keV line which has not been assigned.

major role in it. As a consequence, the spins and parities of the levels of the sideband could not be unambiguously assigned. The position of the $\frac{13}{2}^+$ head of the favored band with respect to the $\frac{3}{2}^-$ ground state is not yet known exactly, since the $\frac{13}{2}^+ \rightarrow \frac{9}{2}^+$ postulated transition has never been observed.[31] From the systematics of the odd-erbium isotopes,[31] one can nevertheless estimate that the approximate excitation energy of this level is about 200 keV.

The results achieved in the present work on ^{157}Er, which, for the favored band, have already been briefly reported previously by us,[17,18] are in good overall agreement with those obtained later by Riley *et al.*[20] who investigated the nuclei $^{157-159}$Er using the ^{116}Cd + ^{48}Ca reaction at 200 MeV. These authors propose a level scheme of ^{157}Er which confirms ours, except that they claim that an additional 803 keV transition exists in the favored band, which they locate between the 766.2 and 809.9 keV transitions (Fig. 7). Our data are not consistent with this proposal. Our coincidence spectrum with a gate on the 810 keV transition [Fig. 5(b) of the present paper] does not allow an 803 keV line with an intensity equal to the one of the 766.2 keV line, as implied by the results of Riley *et al.* Furthermore, our coincidence spectrum for the 807 keV gate [Fig. 5(b)] confirms this conclusion, since it displays very few counts between the 792.5 and 810 keV lines. Consequently, if an 803 keV transition exists in the favored band, it must have a lower relative intensity and so be located higher up in the band than proposed by Riley *et al.*[20] It should be noticed that 801 and 804 keV lines exist in the sideband of ^{157}Er (present paper, Fig. 7, and Ref. 20), which is more strongly populated by the reaction used by Riley *et al.*[20] than by ours, so that a (undetected) connection between the sideband and favored

TABLE I. Properties of the γ-ray transitions measured in the ^{122}Sn + ^{40}Ar(182 MeV) reaction and belonging to the nucleus ^{157}Er. The spin and parity assignments for the transitions in the lower part of the table are tentative as explained in Sec. III A.

$I_i^\pi \rightarrow I_f^\pi$	E_γ (keV)	Int (%)	$I_\gamma(0°)/I_\gamma(90°)$	$I_\gamma(30°)/I_\gamma(90°)$	$\langle M_\gamma \rangle$	Comments
$\frac{17}{2}^+ \rightarrow \frac{13}{2}^+$	266.36±0.03	100.0	1.35±0.08	1.34±0.08	17.9±0.9	
$\frac{21}{2}^+ \rightarrow \frac{17}{2}^+$	414.91±0.03	102.3±2.0	1.31±0.05	1.33±0.05	17.9±0.9	
$\frac{25}{2}^+ \rightarrow \frac{21}{2}^+$	527.36±0.05	94.8±2.0	1.29±0.05	1.41±0.05	17.8±0.9	
$\frac{29}{2}^+ \rightarrow \frac{25}{2}^+$	622.76±0.04	64.9±2.0	1.26±0.12	1.30±0.12	18.7±0.9	
$\frac{33}{2}^+ \rightarrow \frac{29}{2}^+$	703.16±0.05	35.6±3.0	1.67±0.14	1.53±0.12	18.7±1.1	+ ^{156}Er
$\frac{37}{2}^+ \rightarrow \frac{33}{2}^+$	766.21±0.13	30.8±2.0	1.35±0.13	1.26±0.11	17.7±1.0	+ ^{156}Er
$\frac{41}{2}^+ \rightarrow \frac{37}{2}^+$	809.9 ±0.3	25.5±2.0	1.21±0.12	1.31±0.11	19.1±1.2	
$\frac{45}{2}^+ \rightarrow \frac{41}{2}^+$	806.9 ±0.3	17.3±2.0	1.37±0.15	1.20±0.16	21.1±1.7	+ ^{158}Er
$\frac{49}{2}^+ \rightarrow \frac{45}{2}^+$	792.5 ±0.3	29.5±3.0	1.29±0.13	1.32±0.11	20.4±1.2	Doublet
$\frac{53}{2}^+ \rightarrow \frac{49}{2}^+$	834.5 ±0.4	11.8±3.0	1.72±0.56	1.43±0.36	21.4±2.3	
$(\frac{25}{2}^- \rightarrow \frac{25}{2}^+)$	715.5 ±0.2	15.2±2.0	1.32±0.33	1.80±0.25	20.4±3.1	
$(\frac{29}{2}^- \rightarrow \frac{25}{2}^-)$	478.33±0.05	24.2±3.0	1.36±0.11	1.67±0.10	18.1±1.1	
$(\frac{33}{2}^- \rightarrow \frac{29}{2}^-)$	513.97±0.05	35.9±3.0	0.88±0.11	1.14±0.14	17.8±1.1	+ 511 keV
$(\frac{37}{2}^- \rightarrow \frac{33}{2}^-)$	574.73±0.06	20.3±3.0	1.32±0.23	1.94±0.33	20.4±1.2	
$(\frac{41}{2}^- \rightarrow \frac{37}{2}^-)$	651.7 ±0.5	29.4±4.0	1.52±0.52	1.77±0.57	23.1±3.0	Doublet
$(\frac{45}{2}^- \rightarrow \frac{41}{2}^-)$	728.2 ±0.2	27.7±3.0	1.61±0.26	1.83±0.16	19.2±1.2	
$(\frac{49}{2}^- \rightarrow \frac{45}{2}^-)$	801.3 ±0.4	26.3±4.0	2.08±0.45	1.93±0.37	18.7±1.2	
$(\frac{53}{2}^- \rightarrow \frac{49}{2}^-)$	829.0 ±1.0	40.8±5.0	2.02±0.20	1.78±0.29	20.4±1.6	Doublet, + ^{156}Er
$(\frac{57}{2}^- \rightarrow \frac{53}{2}^-)$	804.1 ±0.5	40.0±6.0	1.81±0.32	1.74±0.35	21.3±1.7	+ ^{158}Er

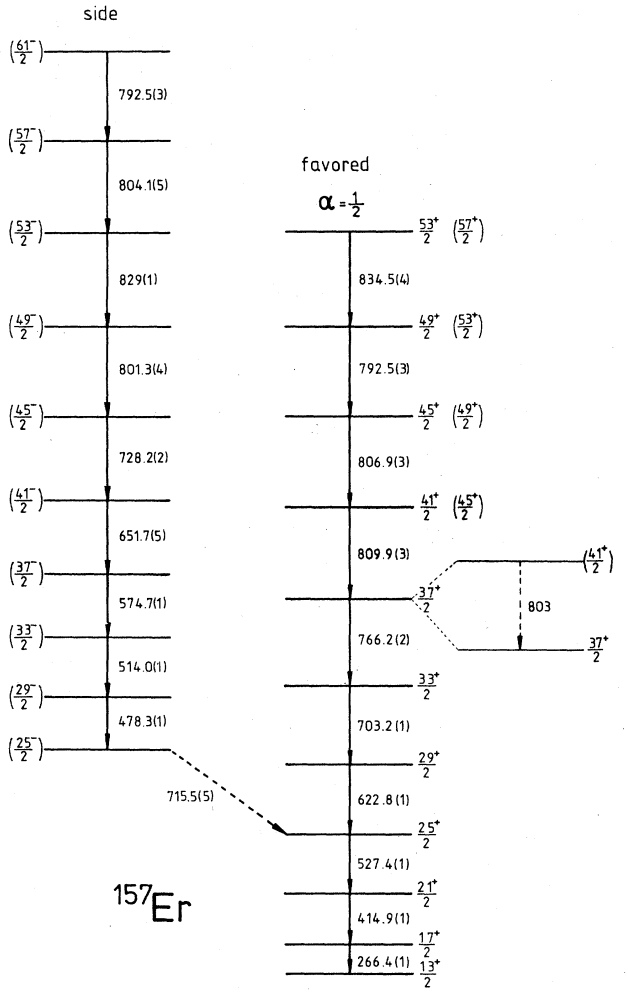

FIG. 7. Partial level scheme of ^{157}Er as obtained in the present experiment. The spin and parity assignments to the levels of the sideband are tentative, and its connection to the favored band is not well established, as discussed in Sec. III A. The position of the 803 keV transition, claimed to exist in the favored band by Riley *et al.* (Ref. 20), is indicated where proposed by the latter authors. The excitation energy of the $\frac{13}{2}^+$ level with respect to the ^{157}Er ground state is not known exactly. The spin and parity assignments to levels of the favored band indicated between parentheses would result from the existence of the 803 keV transition.

band at a higher spin than $\frac{25}{2}^-$ (Fig. 7) could possibly explain the data of Ref. 20. The implications of the possible existence of the 803 keV transition will be discussed in Sec. IV A.

During the experiments described in the present work, data were also obtained on the nucleus ^{158}Er, which has previously been studied by several authors.[1,32] Its yrast band has been observed up to the 38^+ level, above which the feeding intensity suddenly drops dramatically. The results thereby obtained are summarized in Table II. The 40^+ state observed by Burde *et al.*[32] was not confirmed by our experiments. This is in agreement with the results of Riley *et al.*[20]

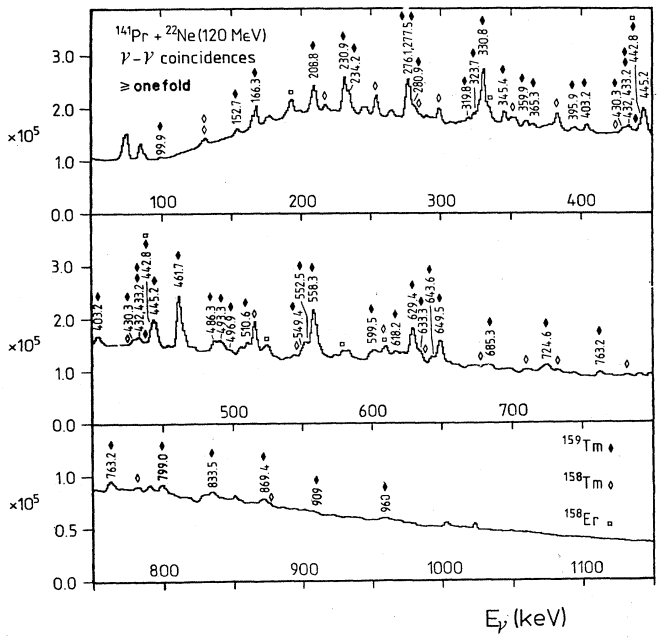

FIG. 8. Total ≥ onefold coincidence spectrum obtained with the ^{141}Pr + ^{22}Ne(120 MeV) reaction. The transitions belonging to ^{158}Er,-^{159}Tm, and ^{158}Tm are also listed in Tables II, III, and V, respectively.

B. The nucleus ^{159}Tm

For the ^{141}Pr + ^{22}Ne reaction, coincidence experiments were carried out at beam energies of 110 and 120 MeV. The total ≥ onefold coincidence spectrum recorded at a bombarding energy of 120 MeV is shown in Fig. 8. The yields for the different reaction channels at this energy were ≅80% for ^{159}Tm, ≅15% for ^{158}Tm, and ≅5% for ^{158}Er (via the 1p4n channel). Angular distributions were measured at a projectile energy of 110 MeV. Accurate transition energies were deduced from this experiment. From the coincidence data, the level scheme proposed previously by Larabee and Waddington[15] could be confirmed and further extended to higher spins. Projected spectra, corresponding to several typical gates placed on transitions in the favored and unfavored bands, are shown in Figs. 9(a) and (b).

Six new transitions appear, at 763.2, 833.5, and 909 keV in the favored band, and at 799.0, 869.5, and 960 keV in the unfavored band. Their energies could be determined most accurately in the sum-gate spectra (Fig. 8), where the corresponding interband low energy transitions at 359.9, 403.2, 395.3, 438, and 432 keV are also weakly present. The intensity ratios $I_\gamma(0°)/I_\gamma(90°)$ and $I_\gamma(30°)/I_\gamma(90°)$, and the angular distribution coefficients A_2 and A_4, confirm the stretched $E2$ nature of the $\Delta I=2$ in-band transitions and the mixed $E2/M1$ nature of the $\Delta I=1$ interband transitions. The order of the new transitions is based on their relative intensities and on accurate energy sums which fulfill the Ritz combination principle. The various results obtained in the nucleus ^{159}Tm are summarized in Table III, and the level scheme thereby establish-

TABLE II. Same as in Table I for the nucleus ^{158}Er.

$I_i^\pi \rightarrow I_f^\pi$	E_γ (keV)	Int (%)	$I_\gamma(0°)/I_\gamma(90°)$	$I_\gamma(30°)/I_\gamma(90°)$	$\langle M_\gamma \rangle$	Comments
$2^+ \rightarrow 0^+$	192.13±0.03	99.9±3.0	1.06±0.05	1.06±0.05	27.0±1.4	
$4^+ \rightarrow 2^+$	335.10±0.03	100.6±2.0	1.19±0.04	1.12±0.04	25.7±1.3	
$6^+ \rightarrow 4^+$	443.13±0.03	100.0	1.36±0.05	1.31±0.04	27.5±1.4	
$8^+ \rightarrow 6^+$	523.14±0.03	99.6±2.0	1.37±0.06	a	24.5±1.3	+ ^{156}Er
$10^+ \rightarrow 8^+$	579.08±0.03	71.2±2.0	1.38±0.15	1.40±0.16	28.1±1.5	+ ^{159}Er
$12^+ \rightarrow 10^+$	608.28±0.04	67.4±2.0	1.31±0.04	1.36±0.06	27.4±1.7	
$14^+ \rightarrow 12^+$	509.75±0.06	57.3±2.0	b	b	24.0±1.3	+ ^{156}Er
$16^+ \rightarrow 14^+$	472.75±0.05	57.4±2.0	1.44±0.07	1.48±0.06	27.5±1.5	
$18^+ \rightarrow 16^+$	566.28±0.05	51.7±2.0	1.38±0.12	1.44±0.13	26.2±1.4	
$20^+ \rightarrow 18^+$	658.89±0.06	53.5±3.0	1.56±0.17	1.59±0.18	24.5±1.5	+ Activity
$22^+ \rightarrow 20^+$	740.42±0.10	35.4±2.0	1.32±0.22	1.35±0.20	26.4±2.1	
$24^+ \rightarrow 22^+$	805.7 ±0.4	34.9±4.0	c	c	21.3±1.7	+ ^{157}Er
$26^+ \rightarrow 24^+$	845.6 ±0.2	25.4±3.0	1.28±0.09	1.09±0.10	28.7±2.4	
$28^+ \rightarrow 26^+$	858.4 ±0.3	26.8±3.0	1.51±0.12	1.73±0.20	25.8±1.7	
$30^+ \rightarrow 28^+$	875.6 ±0.4	19.1±2.0	1.61±0.23	1.60±0.24	27.5±2.0	
$32^+ \rightarrow 30^+$	906.2 ±0.4	20.3±3.0	1.80±0.28	1.86±0.37	25.6±2.3	
$34^+ \rightarrow 32^+$	959.1 ±0.8	15.3±5.0	1.79±0.54	1.44±0.42	27.2±3.5	
$36^+ \rightarrow 34^+$	1019.1 ±0.9	12.5±5.0	1.57±0.46	1.15±0.34	18.4±3.9	
$38^+ \rightarrow 36^+$	1059.2 ±1.5	5.3±2.0	1.27±0.64	1.47±0.68		

[a]Contaminated at 30° by the 511 keV annihilation radiation.
[b]Contaminated at 90° by the 511 keV annihilation radiation.
[c]Contaminated by the 807 keV transition in ^{157}Er.

ed is shown in Fig. 10.

Our results are in very good agreement with the preliminary data of Riedinger *et al.*,[19] who studied this nucleus in a similar but independent experiment. The excitation energy of the $\frac{7}{2}^-$ level with respect to the $\frac{5}{2}^+$ ground state[31] was not known until now. From the systematics of the odd-thulium isotopes,[33] it can be estimated to be $E(\frac{7}{2}^-) \cong 80$ keV.

From our angular distribution measurements, the branching ratios $\lambda(I)$ and the multipole mixing ratios $\delta(I)$ could be deduced for most levels of the favored and unfavored bands with the following definitions:

$$\lambda(I) = \frac{T_\gamma(I \rightarrow I-2)}{T_\gamma(I \rightarrow I-1)} ,$$

$$\delta^2(I) = \frac{T_\gamma(E2, I \rightarrow I-1)}{T_\gamma(M1, I \rightarrow I-1)} .$$

TABLE III. Properties of the γ-ray transitions measured in the ^{141}Pr + ^{22}Ne(120 MeV) reaction and belonging to the nucleus ^{159}Tm. The angular distribution coefficients A_2 and A_4 have been obtained at 110 MeV bombarding energy. The energies of the transition which have not been observed have been inferred from the decay scheme of Fig. 10.

$I_i^\pi \rightarrow I_f^\pi$	E_γ (keV)	Int (%)	$I_\gamma(0°)/I_\gamma(90°)$	$I_\gamma(30°)/I_\gamma(90°)$	A_2	A_4	Comments
$\frac{11}{2}^- \rightarrow \frac{7}{2}^-$	166.31±0.03	79.4±9.9	1.07±0.04	1.10±0.03	0.07±0.02	−0.06±0.04	
$\frac{15}{2}^- \rightarrow \frac{11}{2}^-$	330.80±0.03	100.0	1.38±0.03	1.54±0.04	0.27±0.02	−0.06±0.04	
$\frac{19}{2}^- \rightarrow \frac{15}{2}^-$	461.69±0.03	119.7±2.2	1.43±0.06	1.56±0.06	0.29±0.01	−0.10±0.03	
$\frac{23}{2}^- \rightarrow \frac{19}{2}^-$	558.26±0.03	120.2±7.0	1.52±0.07	1.56±0.08	0.36±0.02	−0.06±0.03	
$\frac{27}{2}^- \rightarrow \frac{23}{2}^-$	629.44±0.03	90.0±5.7	1.55±0.05	1.60±0.04	0.37±0.02	−0.13±0.05	
$\frac{31}{2}^- \rightarrow \frac{27}{2}^-$	649.51±0.03	58.5±3.0	1.39±0.07	1.57±0.08	0.28±0.02	−0.10±0.04	
$\frac{35}{2}^- \rightarrow \frac{31}{2}^-$	486.32±0.04	25.3±1.4	1.37±0.08	1.69±0.12	0.37±0.04	−0.13±0.08	
$\frac{39}{2}^- \rightarrow \frac{35}{2}^-$	510.6 ±0.3	22.5±3.0	a	a	a	a	+ ^{158}Er
$\frac{43}{2}^- \rightarrow \frac{39}{2}^-$	599.5 ±0.1	19.7±1.6	1.42±0.23	1.37±0.19	0.27±0.10	−0.05±0.05	
$\frac{47}{2}^- \rightarrow \frac{43}{2}^-$	685.3 ±0.1	6.5±1.0	1.35±0.23	1.26±0.21	0.25±0.12		
$\frac{51}{2}^- \rightarrow \frac{47}{2}^-$	763.2 ±0.5	6.7±1.0	1.39±0.43	1.81±0.53	0.36±0.16		
$\frac{55}{2}^- \rightarrow \frac{51}{2}^-$	833.5 ±0.6	5.1±2.0	1.79±0.89	1.38±0.55	0.50±0.30		
$\frac{59}{2}^- \rightarrow \frac{55}{2}^-$	909 ±1	<3					Very weak

TABLE III. (*Continued*).

$I_i^\pi \rightarrow I_f^\pi$	E_γ (keV)	Int (%)	$I_\gamma(0°)/I_\gamma(90°)$	$I_\gamma(30°)/I_\gamma(90°)$	A_2	A_4	Comments
$\frac{13}{2}^- \rightarrow \frac{9}{2}^-$	280.9 ±0.2	22.5±1.7	1.26±0.10	1.33±0.10	0.38±0.05	−0.11±0.07	
$\frac{17}{2}^- \rightarrow \frac{13}{2}^-$	445.15±0.03	40.6±2.1	1.45±0.07	1.59±0.08	0.29±0.02	−0.06±0.04	+ ^{158}Er
$\frac{21}{2}^- \rightarrow \frac{17}{2}^-$	549.43±0.03	23.3±1.5	1.43±0.13	1.55±0.14	0.43±0.03	−0.08±0.06	
$\frac{25}{2}^- \rightarrow \frac{21}{2}^-$	618.2 ±0.1	27.3±4.0	1.74±0.12	1.40±0.08	0.27±0.10	−0.12±0.10	
$\frac{29}{2}^- \rightarrow \frac{25}{2}^-$	633.3 ±0.1	19.9±3.1	1.22±0.09	1.27±0.08	0.38±0.08	−0.10±0.08	
$\frac{33}{2}^- \rightarrow \frac{29}{2}^-$	430.3 ±0.1	10.6±1.5	1.45±0.29	1.49±0.30	0.29±0.09	−0.08±0.07	+ ^{158}Tm
$\frac{37}{2}^- \rightarrow \frac{33}{2}^-$	442.82±0.05	15.1±2.5	1.35±0.10	1.42±0.10	0.23±0.04	−0.17±0.07	+ ^{158}Er
$\frac{41}{2}^- \rightarrow \frac{37}{2}^-$	552.5 ±0.1	24.6±2.4	1.52±0.15	1.60±0.17	0.31±0.04	−0.05±0.06	
$\frac{45}{2}^- \rightarrow \frac{41}{2}^-$	643.6 ±0.1	13.8±1.8	1.31±0.10	1.20±0.10	0.29±0.10		
$\frac{49}{2}^- \rightarrow \frac{45}{2}^-$	724.6 ±0.3	15.2±2.0	1.22±0.15	1.41±0.17	0.24±0.08		
$\frac{53}{2}^- \rightarrow \frac{49}{2}^-$	799.0 ±0.3	7.3±2.0	1.43±0.23	1.67±0.32	0.29±0.11		
$\frac{57}{2}^- \rightarrow \frac{53}{2}^-$	869.4 ±0.5	3.1±1.5	1.38±0.39	1.36±0.41	0.24±0.15		
$\frac{61}{2}^- \rightarrow \frac{57}{2}^-$	960 ±1	3.3±1.5	1.33±0.29	1.36±0.28	0.21±0.14		
$\frac{11}{2}^- \rightarrow \frac{9}{2}^-$	50.0 ±0.2						Not observed
$\frac{15}{2}^- \rightarrow \frac{13}{2}^-$	99.9 ±0.3	72.2±15.0	0.57±0.21	0.62±0.27	−0.39±0.20		
$\frac{19}{2}^- \rightarrow \frac{17}{2}^-$	116.4 ±0.2	20.3±4.7					Very weak
$\frac{23}{2}^- \rightarrow \frac{21}{2}^-$	125.0 ±0.1	<15	0.95±0.22	0.75±0.19	−0.03±0.05	−0.14±0.06	
$\frac{27}{2}^- \rightarrow \frac{25}{2}^-$	136.3 ±0.1	<5					Not observed
$\frac{31}{2}^- \rightarrow \frac{29}{2}^-$	152.71±0.06	48.8±11.6	1.05±0.11	0.88±0.08	−0.38±0.09	0.30±0.08	Doublet
$\frac{35}{2}^- \rightarrow \frac{33}{2}^-$	208.78±0.05	62.0±9.9	0.94±0.09	0.92±0.11	−0.03±0.04	0.06±0.06	+ ^{159}Er
$\frac{39}{2}^- \rightarrow \frac{37}{2}^-$	276.1 ±0.2	15.0±5.0	0.77±0.09	0.74±0.07	−0.23±0.08	0.13±0.10	Doublet
$\frac{43}{2}^- \rightarrow \frac{41}{2}^-$	323.7 ±0.1	13.5±3.6	0.88±0.7	1.01±0.08	−0.23±0.09	0.07±0.10	
$\frac{47}{2}^- \rightarrow \frac{45}{2}^-$	365.3 ±0.2	10.7±2.4	1.01±0.12	1.03±0.13	0.02±0.07		
$\frac{51}{2}^- \rightarrow \frac{49}{2}^-$	403.2 ±0.3	7.4±2.0	1.04±0.11	1.07±0.10	0.04±0.07		
$\frac{55}{2}^- \rightarrow \frac{53}{2}^-$	438 ±1	4.6±1.5	0.85±0.16	1.50±0.30	0.16±0.09		
$\frac{59}{2}^- \rightarrow \frac{57}{2}^-$	477 ±2						Not observed
$\frac{9}{2}^- \rightarrow \frac{7}{2}^-$	116.4 ±0.2	<5					Doublet
$\frac{13}{2}^- \rightarrow \frac{11}{2}^-$	230.93±0.03	75.4±6.1	1.76±0.05	1.53±0.04	0.26±0.03	0.17±0.05	
$\frac{17}{2}^- \rightarrow \frac{15}{2}^-$	345.35±0.04	31.6±2.5	1.49±0.05	1.55±0.07	0.26±0.03	0.02±0.06	
$\frac{21}{2}^- \rightarrow \frac{19}{2}^-$	433.22±0.05	18.3±1.8	1.49±0.18	1.56±0.19	0.15±0.04	−0.05±0.10	Doublet
$\frac{25}{2}^- \rightarrow \frac{23}{2}^-$	493.3 ±0.2	21.5±2.4	1.32±0.13	1.68±0.15	0.25±0.07	0.01±0.10	
$\frac{29}{2}^- \rightarrow \frac{27}{2}^-$	496.9 ±0.1	10.2±1.6	1.05±0.18	1.23±0.18	0.13±0.10	−0.24±0.15	
$\frac{33}{2}^- \rightarrow \frac{31}{2}^-$	277.5 ±0.1	48.4 ±5.6	0.77±0.09	0.74±0.07	−0.23±0.08	0.13±0.10	
$\frac{37}{2}^- \rightarrow \frac{35}{2}^-$	234.2 ±0.1	46.4±6.1	0.88±0.04	0.96±0.05	−0.25±0.03	0.03±0.04	
$\frac{41}{2}^- \rightarrow \frac{39}{2}^-$	276.1 ±0.2	15.0±5.0	0.77±0.09	0.74±0.07	−0.23±0.08	0.13±0.10	Doublet
$\frac{45}{2}^- \rightarrow \frac{43}{2}^-$	319.8 ±0.2	9.3±3.6	0.64±0.26	0.99±0.26	−0.09±0.10	−0.36±0.21	
$\frac{49}{2}^- \rightarrow \frac{47}{2}^-$	359.9 ±0.3	6.0±2.1	1.01±0.12	1.10±0.15	0.09±0.07	−0.22±0.13	
$\frac{53}{2}^- \rightarrow \frac{51}{2}^-$	395.9 ±0.4	3.0±1.6	0.88±0.33	1.07±0.36			
$\frac{57}{2}^- \rightarrow \frac{55}{2}^-$	432 ±1	<2					Doublet
$\frac{61}{2}^- \rightarrow \frac{59}{2}^-$	483 ±2						Not observed

[a]Contaminated by the 511 keV annihilation radiation.

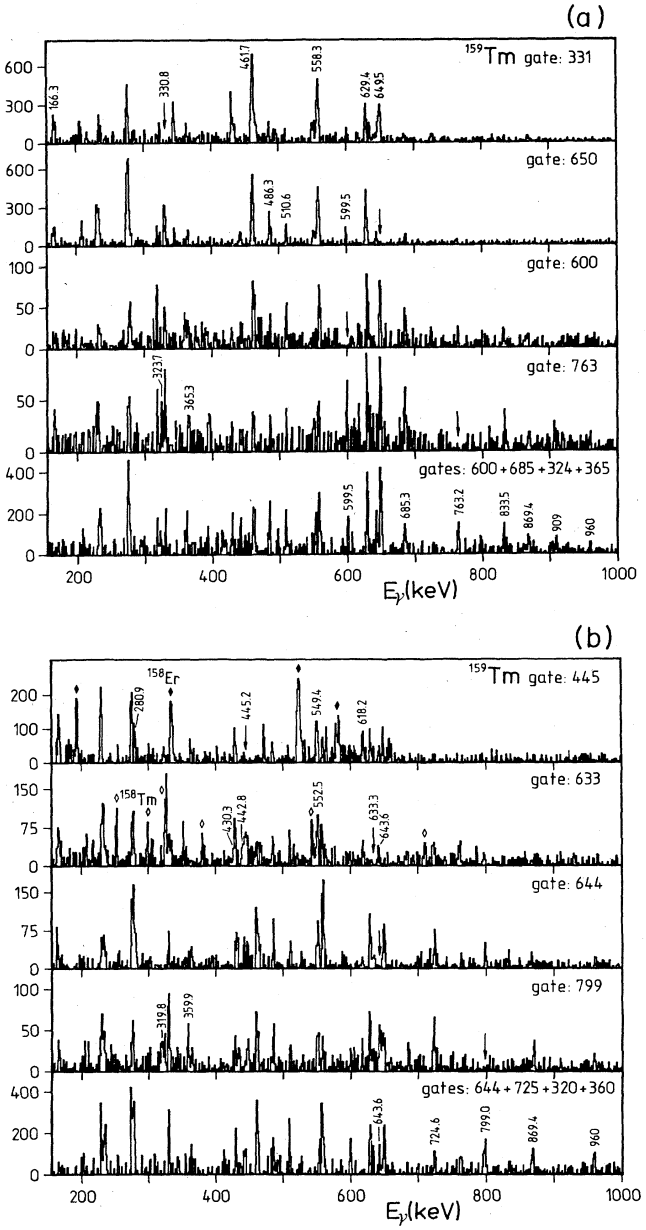

FIG. 9. Coincidence projections obtained with the ^{141}Pr(^{22}Ne,4n)^{159}Tm reaction at $E(^{22}\text{Ne})=120$ MeV. The gates are marked by arrows in each spectrum. Transitions belonging to ^{158}Er and ^{158}Tm are indicated by solid and open diamonds, respectively. The other transitions belong to ^{159}Tm and are also listed in Table III.

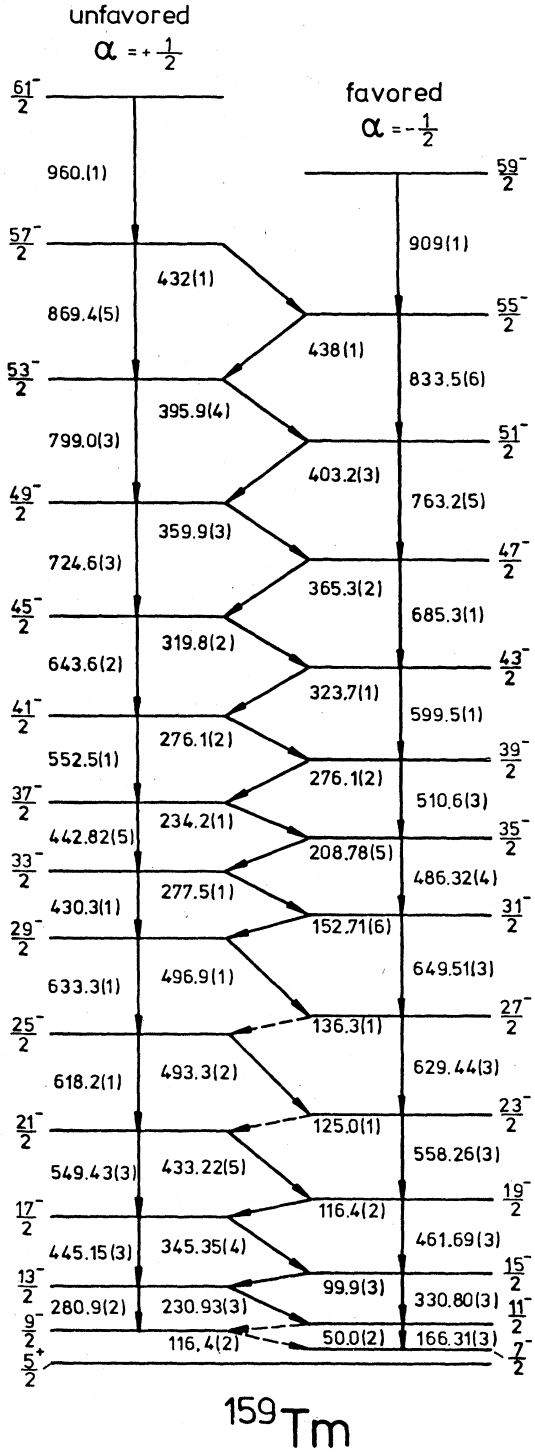

FIG. 10. Partial level scheme of ^{159}Tm as obtained in the present experiment. The excitation energy of the $\frac{7}{2}^-$ level with respect to the ^{159}Tm ground state is not known exactly.

Using these quantities, the ratio $B(M1)/Q_0^2$ could be computed, in the framework of the strong coupling limit,[34] from the following expression:

$$\frac{B(M1)}{Q_0^2}=6.93\times10^{-8}\frac{\langle IK20\,|\,I-2K\rangle^2}{\lambda(I)[1+\delta^2(I)]}\frac{E_\gamma^5(\Delta I=2)}{E_\gamma^3(\Delta I=1)},$$

where the transition energies are given in keV and Q_0 is the electric quadrupole moment in 10^{-24} cm^2. In the strong coupling limit, $B(M1)$ is proportional to $(g_K-g_R)^2$, where g_K and g_R are the single-particle and collective gyromagnetic ratios, respectively. The values of $\lambda(I)$, $\delta(I)$, and $B(M1)/Q_0^2$ are listed in Table IV. Figure 11 displays the ratio $B(M1)/Q_0^2$ as a function of the spin of the emitting level for the two observed bands. The nu-

TABLE IV. Decay properties of the various levels in ^{159}Tm. For each level, the following are given: the total photon intensities of the transitions deexciting it with the normalization of Table III; the branching ratio $\lambda(I)$ and multipole mixing ratio $|\delta(I)|$ defined in Sec. III B; and the quantity $B(M1)/Q_0^2$ which can be deduced from them as outlined in Sec. III B.

I^π	Int(I)	$\lambda(I)$	$\lvert\delta(I)\rvert$	$B(M1)/Q_0^2$	Comments
$\frac{11}{2}^-$	>80.0	a	a	a	
$\frac{15}{2}^-$	172.2±15.0	5.4 ±1.9	<0.40	0.008 ±0.003	
$\frac{19}{2}^-$	140.0±5.2	18.8 ±6.9	0.35±0.25	0.009 ±0.004	
$\frac{23}{2}^-$	<135.0	23.9 ±8.8	<0.10	0.022 ±0.006	
$\frac{27}{2}^-$	<95.0	b	b	b	
$\frac{31}{2}^-$	107.3±12.4	3.2 ±0.2	<0.20	0.21 ±0.02	
$\frac{35}{2}^-$	87.3±10.0	0.62±0.06	0.13±0.02	0.11 ±0.01	
$\frac{39}{2}^-$	37.5±6.0	c	c	c	
$\frac{43}{2}^-$	33.2±3.9	1.42±0.12	<0.20	0.04 ±0.01	
$\frac{47}{2}^-$	17.2±2.6	0.69±0.10	<0.20	0.10 ±0.02	
$\frac{51}{2}^-$	14.1±2.2	1.1 ±0.3	0.17±0.07	0.09 ±0.03	
$\frac{55}{2}^-$	9.7±2.6	0.5 ±0.2			Very weak
$\frac{59}{2}^-$	<5.0				Very weak
$\frac{13}{2}^-$	97.9±6.3	0.41±0.02	0.32±0.02	0.0029±0.0002	
$\frac{17}{2}^-$	72.2±3.3	1.42±0.06	0.36±0.03	0.0040±0.0002	Very weak
$\frac{21}{2}^-$	41.6±2.3	1.35±0.10	0.23±0.02	0.0078±0.0007	
$\frac{25}{2}^-$	48.8±4.7	0.97±0.07	0.34±0.07	0.0140±0.0012	
$\frac{29}{2}^-$	30.1±3.5	1.88±0.21	<0.20	0.0090±0.0011	
$\frac{33}{2}^-$	59.0±5.3	0.24±0.03	<0.10	0.064 ±0.009	
$\frac{37}{2}^-$	62.5±6.4	0.39±0.02	0.08±0.02	0.075 ±0.005	
$\frac{41}{2}^-$	29.6±5.5	0.72±0.09	<0.10	0.078 ±0.008	
$\frac{45}{2}^-$	23.1±4.0	1.25±0.19	0.08±0.04	0.063 ±0.010	
$\frac{49}{2}^-$	21.1±2.9	2.8 ±0.3	0.2 ±0.1	0.036 ±0.006	
$\frac{53}{2}^-$	10.3±2.6	2.7 ±0.5	<0.20	0.043 ±0.009	
$\frac{57}{2}^-$	<5.1				Very weak
$\frac{61}{2}^-$	<4.0				Very weak

[a] $\frac{11}{2}^- \rightarrow \frac{9}{2}^-$ not observed.
[b] $\frac{27}{2}^- \rightarrow \frac{25}{2}^-$ not observed.
[c] $\frac{39}{2}^- \rightarrow \frac{35}{2}^-$ contaminated by the 511 keV annihilation radiation.

cleus ^{159}Tm has a similar behavior for this quantity as its isotone ^{157}Ho.[34] This will be further discussed in Sec. IV C 2.

In the experiments described here, some information on high spin states in the odd-odd nucleus ^{158}Tm has also been obtained (Table V). The proposed level scheme is reproduced in Fig. 12. The previous knowledge on this nucleus[35] has been extended from level 19^- up to level 23^-, and, perhaps, 25^-. At 120 MeV bombarding energy, the nucleus ^{158}Tm is only weakly populated in the ^{141}Pr + ^{22}Ne reaction; a more complete investigation of ^{158}Tm should be carried out at a higher beam energy.

IV. DISCUSSION

A. Experimental Routhians and alignment

For several years most of the data obtained on the high-spin members of rotational bands in deformed nuclei have been interpreted in the framework of the cranked shell model (CSM) developed by Bengtsson and Frauendor.[12,16] As discussed by these authors, from the information contained in the level scheme, it is possible to obtain "experimental" values for the excitation energy $E'(I)$ in the rotating frame

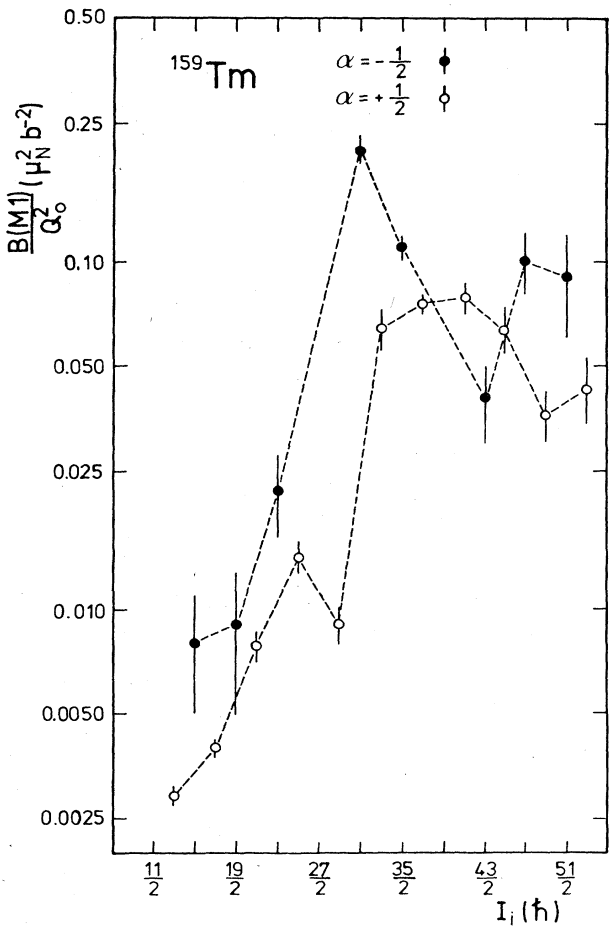

FIG. 11. Experimental values of $B(M1,I\rightarrow I-1)/Q_0^2$ as a function of I for the transitions in the favored ($\alpha=-\frac{1}{2}$, solid circles) and unfavored ($\alpha=+\frac{1}{2}$, open circles) bands in ^{159}Tm, deduced as outlined in Sec. III B.

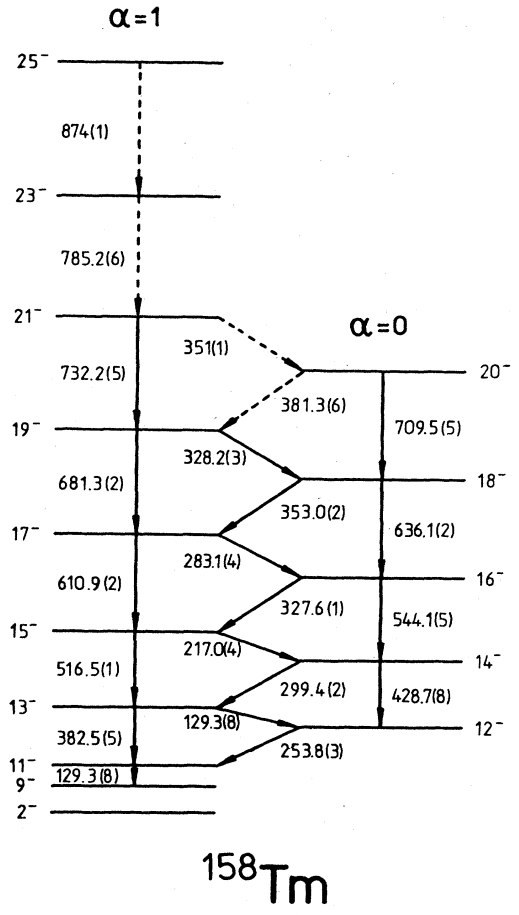

FIG. 12. Partial level scheme of ^{158}Tm as obtained in the present experiment, supplemented by data of Ref. 35.

$$E'(I)=E(I)-\omega(I)\cdot I_x(I)$$

and for the projection $I_x(I)$ of the angular momentum I on the axis of rotation

$$I_x(I)=[(I+\tfrac{1}{2})^2-K^2]^{1/2}\ .$$

K is the projection of I on the nuclear symmetry axis. The rotational frequency $\omega(I)$ is given by $\hbar\omega(I)\cong\frac{1}{2}E_\gamma(I\rightarrow I-2)$, valid for $I\gg K$.

The intrinsic excitation energy in the rotating frame $e'(I)$ and the aligned angular momentum projection $i_x(I)$ can be obtained by subtracting, from $E'(I)$ and $I_x(I)$, the collective parts of the excitation energy and of the angular momentum projection, respectively. In order to do this, it is convenient to define a reference frame. Two choices of reference frames are of common use: either the ground-state band of an even-even nucleus (g reference), or its yrast band (yrast reference). These references are appropriate for the corresponding even-even nucleus. For odd-N and odd-Z nuclei, the intrinsic energies are referred to the average of the reference configurations of the neighboring even-even nuclei, and the pairing gap (estimated from the odd-even mass difference) is added. The various reference configurations are discussed in detail by Bengtsson *et al.*[36]

The ground-state band of even-even nuclei is usually not known above the first band crossing, so that the g reference has to be extrapolated to higher rotational frequencies by appropriate expressions. This is generally done using the parametrization of Harris[37] for the nuclear moment of inertia

$$\mathcal{I}=\mathcal{I}_0+\omega^2\mathcal{I}_1\ .$$

The parameters $\mathcal{I}_0$ and $\mathcal{I}_1$ are determined by a fit to the g-band values of $I_x(I)$, using

$$I_x(\omega)=\mathcal{I}\omega=\omega\mathcal{I}_0+\omega^3\mathcal{I}_1\ .$$

This procedure can be extended to odd-A nuclei with the help of a three-parameter fit to some rotational band, the favored band, for instance (this is the so-called "adapted g reference"),

$$I_x(\omega)=\omega\mathcal{I}_0+\omega^3\mathcal{I}_1+i\ .$$

The aligned angular momentum i of this band is assumed

TABLE V. Same as in Table III for the nucleus ^{158}Tm.

$I_i^\pi \rightarrow I_f^\pi$	E_γ (keV)	Int (%)	$I_\gamma(0°)/I_\gamma(90°)$	$I_\gamma(30°)/I_\gamma(90°)$	Comments
$11^- \rightarrow 9^-$	129.3±0.8	243.0±15.0	a	a	Doublet
$13^- \rightarrow 11^-$	382.5±0.5	100.0	1.52±0.38	1.64±0.41	
$15^- \rightarrow 13^-$	516.5±0.1	139.3±9.0	b	b	
$17^- \rightarrow 15^-$	610.9±0.2	97.9±6.0	1.47±0.13	1.56±0.12	
$19^- \rightarrow 17^-$	681.3±0.2	53.8±6.0	1.38±0.22	1.43±0.23	
$21^- \rightarrow 19^-$	732.2±0.5	60.0±6.0	1.39±0.21	1.73±0.31	
$23^- \rightarrow 21^-$	785.2±0.6	32.4±4.0	1.37±0.23	1.42±0.21	
$25^- \rightarrow 23^-$	874 ±1	27.9±7.0	1.27±0.26	1.29±0.25	
$14^- \rightarrow 12^-$	428.7±0.8	c	c	c	
$16^- \rightarrow 14^-$	544.1±0.5	39.6±4.0	1.48±0.20	1.78±0.26	
$18^- \rightarrow 16^-$	636.1±0.2	<25			Very weak
$20^- \rightarrow 18^-$	709.5±0.5	49.4±6.0	1.44±0.17	1.30±0.22	
$13^- \rightarrow 12^-$	129.3±0.8	d	a	a	Doublet
$15^- \rightarrow 14^-$	217.0±0.4	60.2±7.0	0.84±0.11	0.95±0.16	
$17^- \rightarrow 16^-$	283.1±0.4	53.1±8.0	0.54±0.12	0.67±0.16	
$19^- \rightarrow 18^-$	328.2±0.3	25	1.10±0.08	0.90±0.07	Doublet
$21^- \rightarrow 20^-$	350.9±0.8	<20			Very weak
$12^- \rightarrow 11^-$	253.8±0.3	159.0±11.0	0.89±0.07	1.17±0.11	
$14^- \rightarrow 13^-$	299.4±0.2	83.9±6.0	0.95±0.06	1.18±0.10	
$16^- \rightarrow 15^-$	327.6±0.1	102.0±9.0	1.10±0.08	0.90±0.07	Doublet
$18^- \rightarrow 17^-$	353.0±0.2	48.1±5.0	0.61±0.12	1.11±0.23	
$20^- \rightarrow 19^-$	381.3±0.6	<15			Very weak

[a]Contaminated at 90° by an activity peak.
[b]Contaminated at 90° by the 511 keV annihilation radiation.
[c]Contaminated by the 430.3 keV transition in ^{159}Tm.
[d]Unresolved doublet.

TABLE VI. Parameters used in the CSM analysis of the experimental data on the indicated nuclei, determined as outlined in Sec. IV A. For each nucleus, the following are given: the parameters $\mathcal{I}_0$ and $\mathcal{I}_1$ of the reference configuration; the pairing gap parameters Δ_n and Δ_p; and the assumed value for the K quantum number of the bands. The latter are the ground-state band for the even-even nuclei; the favored positive parity band for the odd-A Er nuclei; the favored and unfavored negative parity bands in ^{157}Ho and ^{159}Tm; and the $(\nu i_{13/2})(\pi h_{11/2})$ band in ^{158}Tm.

	Nucleus	$\mathcal{I}_0$ (MeV$^{-1}\hbar^2$)	$\mathcal{I}_1$ (MeV$^{-3}\hbar^4$)	Δ_n (MeV)	Δ_p (MeV)	K ($\hbar$)
$Z=68$	^{156}Er	8.0	130.0	1.24	1.38	0
	^{157}Er	16.0	105.0	1.38	1.28	$\frac{1}{2}$
	^{158}Er	18.5	85.0	1.35	1.18	0
	^{159}Er	23.5	92.5	1.23	1.21	$\frac{3}{2}$
	^{160}Er	23.0	83.0	1.21	1.23	0
	^{161}Er	28.0	90.0	1.13	1.15	$\frac{3}{2}, \frac{5}{2}$
$N=90$	^{158}Er	18.5	85.0	1.35	1.18	0
	^{159}Tm	22.0	80.0	1.29	1.30	$\frac{7}{2}$
	^{160}Yb	17.0	92.0	1.23	1.24	0
	^{158}Tm	10.5	148.0	1.31	1.38	$\frac{1}{2}+\frac{7}{2}=4$

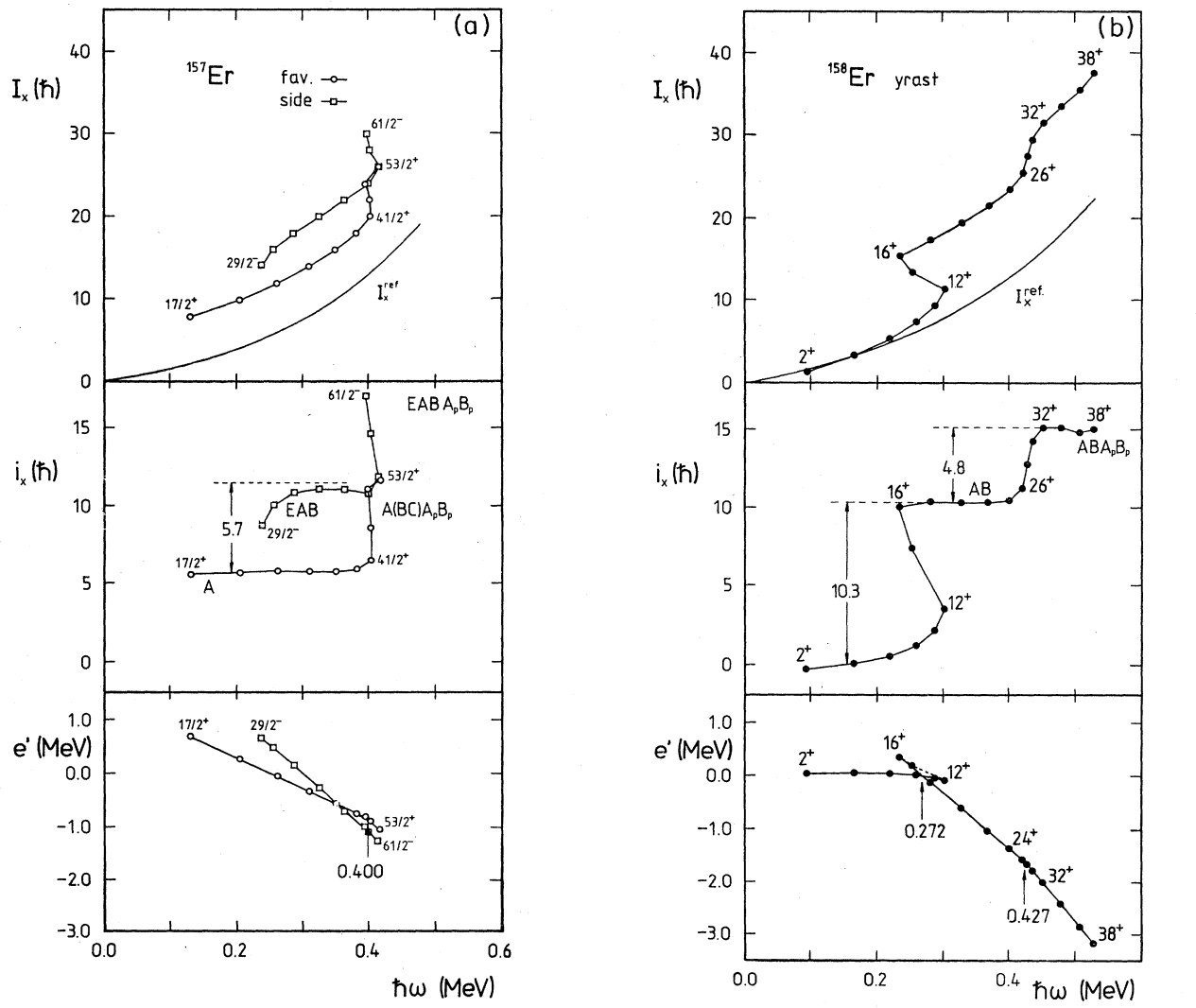

FIG. 13. Plots of the quantities I_x, i_x, and e' vs $\hbar\omega$, defined and deduced as outlined in Sec. IV A, for the favored and sidebands in ^{157}Er (a), for the yrast band in ^{158}Er (b), for the favored ($\alpha=-\frac{1}{2}$) and unfavored ($\alpha=+\frac{1}{2}$) bands in ^{159}Tm (c), and for the yrast band in ^{158}Tm (d). The critical frequencies $\hbar\omega_c$ for the various alignments are marked by arrows in the e' diagrams, and the corresponding alignment gains Δi_x are indicated in the i_x diagrams. The labels A, B, C, E, A_p, and B_p refer to quasiparticle trajectories in the CSM calculations described in Sec. IV B, and correspond to the quasiparticle diagrams of Figs. 15 and 18. The references used for the calculations of I_x^{ref} are described in Sec. IV A, and the corresponding parameters are given in Table VI.

to be constant in the considered range of ω. The reference angular momentum projection, I_x^{ref}, and excitation energy, E'_{ref}, are then given by[12]

$$I_x^{ref}(\omega)=\omega(\mathcal{I}_0+\omega^2\mathcal{I}_1)\ ,$$

$$E'_{ref}(\omega)=-\tfrac{1}{2}\omega^2\mathcal{I}_0-\tfrac{1}{4}\omega^4\mathcal{I}_1+\frac{\hbar^2}{8\mathcal{I}_0}\ .$$

Finally, the projection of the aligned angular momentum, $i_x(\omega)$, and the intrinsic excitation energy, $e'(\omega)$, take the following values:

$$i_x(\omega)=I_x(\omega)-I_x^{ref}(\omega)\ ,$$

$$e'(\omega)=E'(\omega)-E'_{ref}(\omega)\ .$$

The various rotational bands investigated in the nuclei ^{157}Er, ^{158}Er, ^{159}Tm, and ^{158}Tm during the course of the present work have been analyzed according to the procedure already outlined. Table VI summarized the moment of inertia parameters $\mathcal{I}_0$ and $\mathcal{I}_1$, the pairing gaps Δ_n and Δ_p, and the K values used in our analysis. The parameters $\mathcal{I}_0$ and $\mathcal{I}_1$ were determined by a fit of I_x for the g band in the case of even-even nuclei and for the low-spin part (i.e., below the first crossing) of the favored band in the case of odd-A and odd-odd nuclei. The pairing potential parameters Δ_n and Δ_p were deduced from the experimental odd-even mass differences;[38] a four-point interpolation formula proposed by Bengtsson *et al.*[36] was used, and the extra binding energy of odd-odd nuclei due to the residual interaction between the unpaired neutron and proton[39] was taken into account.

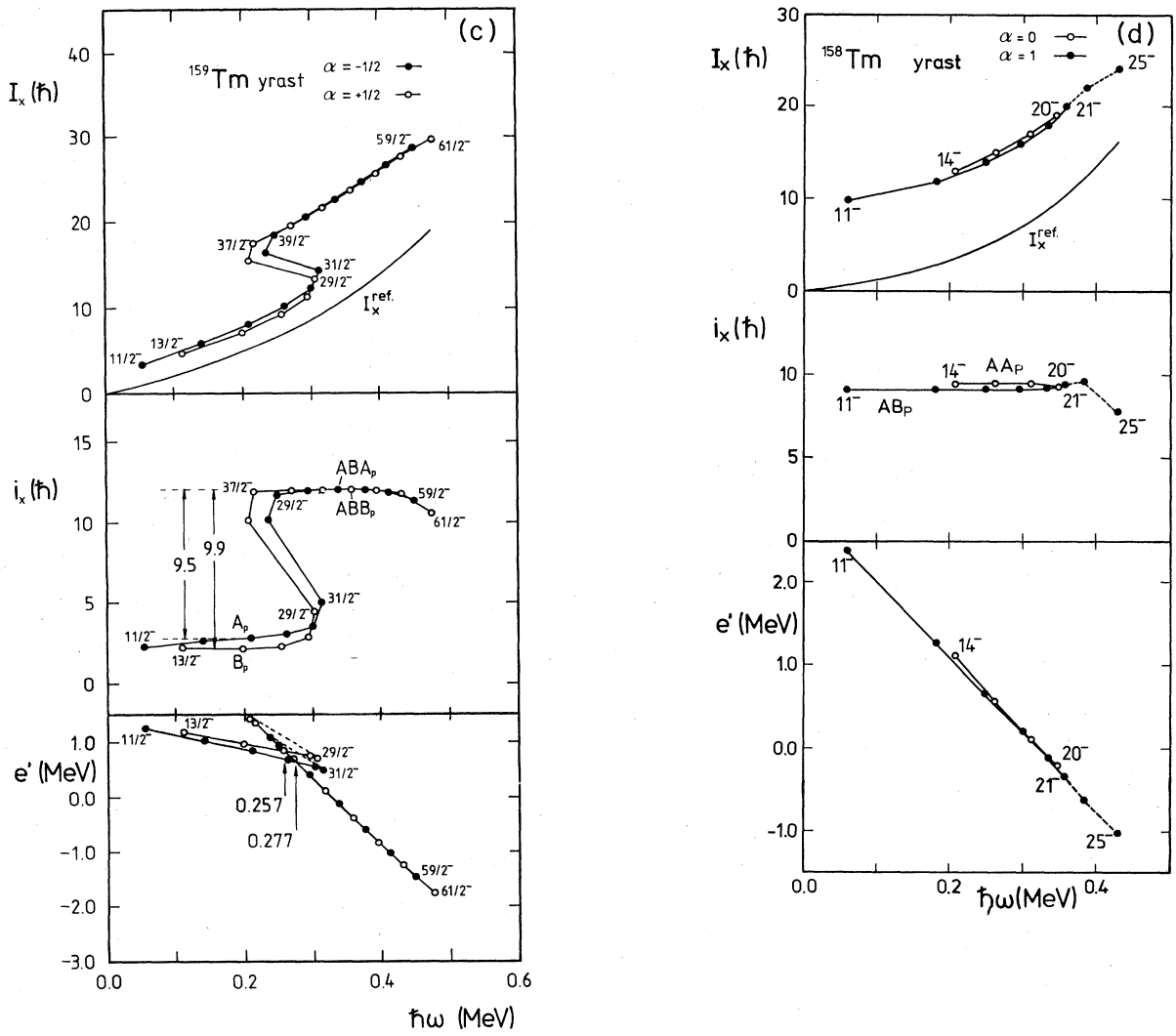

FIG. 13. (*Continued*).

The experimental functions $I_x(\omega)$, $i_x(\omega)$, and $e'(\omega)$ are shown in Figs. 13(a)—(d) for the investigated nuclei, together with the corresponding reference configurations. From the $i_x(\omega)$ plots, it clearly appears that both the favored band and the sideband studied in the odd-N nucleus ^{157}Er display a sharp upbending at a rotational frequency $\hbar\omega = 0.40$ MeV, whereas such an effect is absent in the favored and unfavored bands of the odd-Z nucleus ^{159}Tm at high rotational frequency, i.e., between 0.28 and 0.48 MeV. On the other hand, a first backbending is observed in the favored and unfavored bands of ^{159}Tm around $\hbar\omega = 0.27$ MeV, but not in the favored band of ^{157}Er. The crossing frequencies, $\hbar\omega_c$, and the gains in aligned angular momentum, ΔI_x, are also indicated in Fig. 13.

The yrast bands of ^{157}Er and ^{159}Tm are compared in Fig. 14 with the yrast bands of the even-even nuclei ^{156}Er and ^{158}Er ($Z=68$ isotopes), and of ^{158}Er and ^{160}Yb ($N=90$ isotones), respectively. From this figure, one can definitely conclude that, in the favored band of ^{157}Er, the odd $i_{13/2}$ neutron does block the first alignment observed in the neighboring even-even nuclei, but that it does not do so for the second one; in the favored and unfavored bands of ^{159}Tm, the odd $h_{11/2}$ proton does not hinder the first alignment, but it does prevent the second one. This behavior can be understood if one assumes that the first backbending is due to the rotation alignment (RAL) of a pair of $i_{13/2}$ neutrons, as already shown earlier by Grosse, Stephens, and Diamond,[9,10] and that the second backbending is produced by the RAL of a pair of $h_{1/2}$ protons, in agreement with the predictions of Faessler and Ploszajczak[6] and with the results of CHFB (Ref. 11) and CSM (Ref. 12) calculations. The experimental determination of the proton nature of the second backbending in ^{158}Er, which was first suggested on the basis of data on ^{159}Tm alone,[17,19] has been definitely established by the simultaneous consideration of ^{157}Er and ^{159}Tm (Ref. 18), and later confirmed by results obtained on $^{157-159}$Er (Ref. 20).

It follows from this that the two bands observed in the odd-odd nucleus ^{158}Tm should not display neither the first nor the second backbending, since they are believed to be

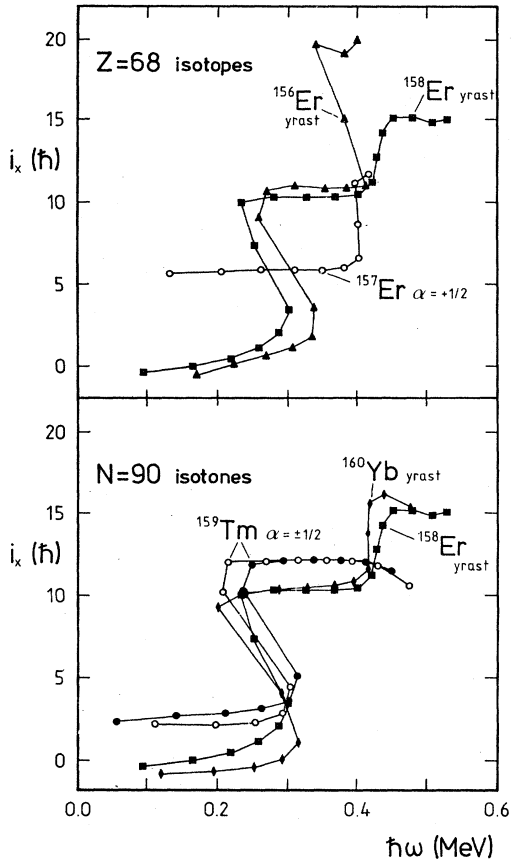

FIG. 14. Comparison between the alignment plots of i_x vs $\hbar\omega$ (defined in Sec. IV A), for the $Z=68$ isotopes (yrast bands in ^{156}Er, triangles; ^{158}Er, squares; and favored band in ^{157}Er, circles), and for the $N=90$ isotones (yrast bands in ^{158}Er, squares; ^{160}Yb, diamonds; favored and unfavored bands in ^{159}Tm, solid and open circles, respectively).

built on a $(\nu i_{13/2})$ $(\pi h_{11/2})$ configuration.[35] In the present work, the absence of the neutron alignment has been confirmed [see Fig. 13(d)]; further experiments extending the knowledge of this nucleus to higher rotational frequencies are, however, necessary to check whether or not the proton alignment is also blocked in this nucleus.

It should finally be noticed that, if the additional 803 keV transition proposed by Riley *et al.*[20] in the favored band of ^{157}Er (See Sec. III A) would indeed be present, the critical frequency $\hbar\omega_c$ for the proton alignment in this nucleus would not be modified (as well as the conclusion[18] on the proton nature of the second backbending near $N=90$). The corresponding rise in angular momentum Δi_x would, however, be increased by approximately $2\hbar$ with respect to the results of the present work.

B. Comparison with CSM calculations

The experimental aligned angular momentum $i_x(\omega)$ and intrinsic excitation energy $e'(\omega)$ can be compared with the corresponding theoretical predictions obtained by the diagonalization of the cranked shell model Hamiltonian[12,16]

$$h_{\mathrm{CSM}}=h_{\mathrm{sp}}-\Delta(P^{+}+P)-\lambda\hat{N}-\omega\hat{j}_x \ .$$

In this expression, h_{sp} is the single particle Hamiltonian; P^{+} (P) creates (annihilates) the pair field, the strength of which is fixed by the gap parameter Δ; λ is the chemical potential, which determines the expectation value of the particle number operator $\hat{N}$; and $\hat{j}_x$ is the single-particle angular momentum operator. From the eigenstates of h_{CSM}, configurations of independent quasiparticles can be constructed. The underlying theory has been developed in full detail elsewhere.[12,16,40]

The parameters used in our CSM calculations are listed in Table VII. The quadrupole deformation parameter ϵ_2 has been estimated from experimental transition electric quadrupole moments derived from lifetime data,[41,42] except for the nucleus ^{159}Tm for which an average value between ^{158}Er and ^{160}Yb has been used, because no experimental data are so far available. The hexadecapole deformation ϵ_4 is expected to be small in the $A\cong 158$ mass region, and theoretical values[43] have been used. Except for ^{159}Tm, the triaxial deformation γ has been taken equal to zero. The pairing gap parameters Δ_n and Δ_p have been estimated from odd-even mass differences as outlined in Sec. IV A. As we were mainly interested in the behavior of the proton A_pB_p crossing and of the neutron BC and AD crossings, in our CSM calculations we have used reduced neutron pairing gaps ($\Delta_n=0.8\ \Delta_{oe}$) to account for

TABLE VII. Parameters used in the CSM calculations on the indicated nuclei, carried out as described in Sec. IV B. The quantity $\hbar\omega_0$ is 41.2 $A^{-1/3}$ MeV.

Nucleus	N	Z	$\hbar\omega_0$ (MeV)	ϵ_2	ϵ_4	γ (deg)	$\Delta_n/\hbar\omega_0$[b]	$\Delta_p/\hbar\omega_0$	$\lambda_n/\hbar\omega_0$	$\lambda_p/\hbar\omega_0$
^{156}Er	88	68	7.653	0.162	−0.020	0	0.130	0.180	6.371	5.799
^{157}Er	89	68	7.637	0.201	−0.020	0	0.145	0.163	6.357	5.807
^{158}Er	90	68	7.621	0.218	−0.020	0	0.142	0.156	6.365	5.815
^{159}Er	91	68	7.605	0.241	−0.020	0	0.130	0.159	6.372	5.815
^{160}Er	92	68	7.589	0.243	−0.020	0	0.127	0.162	6.395	5.816
^{161}Er	93	68	7.573	0.247	−0.015	0	0.119	0.152	6.418	5.817
^{162}Er	94	68	7.558	0.255	−0.010	0	0.114	0.142	6.436	5.815
^{159}Tm	90	69	7.605	0.200[a]	−0.015	−20	0.136	0.171	6.391	5.829

[a]Average value for ^{158}Er and ^{160}Yb.

[b]Reduced by 20% in order to reproduce the BC and AD crossings.

the reduction of the pairing correlations due to the presence of several aligned neutrons.[36] The Fermi levels λ_n and λ_p have been adjusted in order to reproduce, on the average, the correct particle numbers. All parameters have been kept constant as a function of the rotational frequency $\hbar\omega$, in accordance with one of the main assumptions of the CSM theory.

The diagonalization of h_{CSM} yields the quasiparticle energies, which can be plotted vs $\hbar\omega$, yielding the so-called Bengtsson-Frauendorf or quasiparticle diagrams, shown in Figs. 15 and 18 for the nuclei ^{157}Er and ^{159}Tm, respectively. The levels are marked according to the usual conventions.[36] From the quasiparticle diagrams, the crossing frequencies $\hbar\omega_c$, the aligned angular momenta $i_x = -(de'/d\omega)$, and the strength of the interaction between crossing levels $|V|$ can be read and compared with the experimental values.

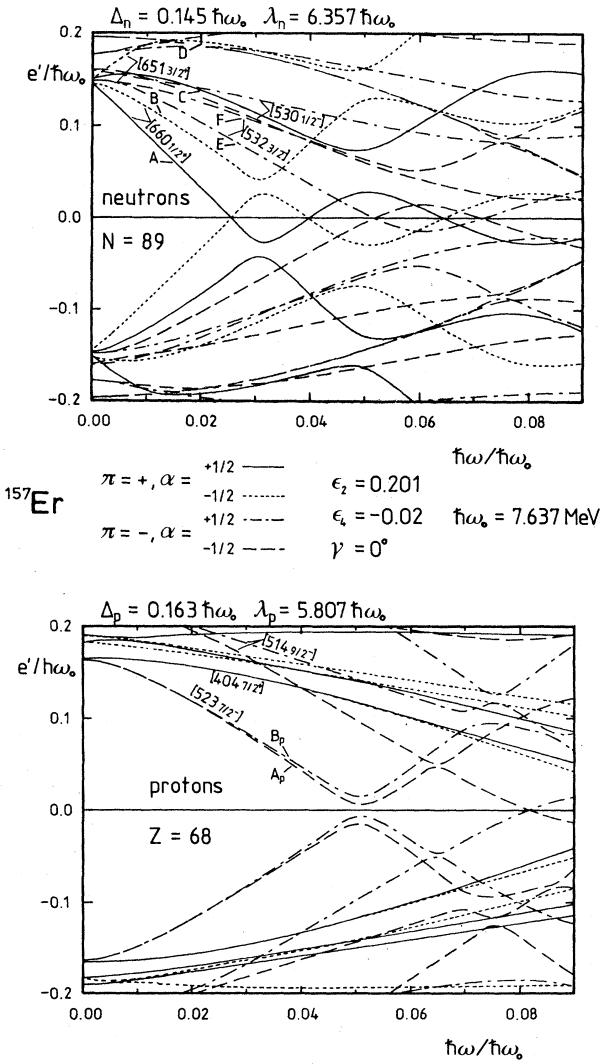

FIG. 15. Quasiparticle diagrams for neutrons (upper) and protons (lower) in ^{157}Er, calculated as outlined in Sec. IV B, with the parameters given in the figure and listed in Table VII. The corresponding Nilsson configurations at $\hbar\omega = 0$ are indicated by their asymptotic quantum numbers.

At the beginning of the rare earth region, the *s* band in even-even nuclei is understood as a two-quasineutron excitation (*AB*), whereas the favored and unfavored bands in odd-*N* nuclei are, at low spin, one quasineutron excitations, marked (*A*) and (*B*), respectively. In odd-*Z* nuclei of the same region, the favored and unfavored bands correspond, at low spin, to one-quasiproton excitations, marked (A_p) and (B_p), respectively. The most probable quasiparticle configurations corresponding to the various bands investigated in the present work are indicated in Fig. 13, with the notations of Figs. 15 and 18.

The level crossings that could be responsible for the upbending observed at $\hbar\omega_c = 0.40$ MeV in the favored band of ^{157}Er are (1) the A_pB_p proton crossing, and (2) the *BC* neutron crossing. In order to determine whether or not the latter neutron crossing contributes to this upbending, CSM calculations have been carried out for a series of erbium isotopes $^{156-162}$Er, and the results have been compared with the available experimental data.[44,4,1,32,20,45] The calculated and, when available, experimental crossing frequencies, aligned angular momentum gains, and interaction strengths are given in Fig. 16 for the A_pB_p proton crossing, and in Fig. 17 for the *BC* and *AD* neutron crossings. In the case of ^{156}Er, we have assumed, in analogy with ^{158}Er, that the second backbending in the yrast band[4] and the first backbending in the negative parity band[44] are due to the A_pB_p and *BC* crossings, respectively. There is a fair agreement between the experimental

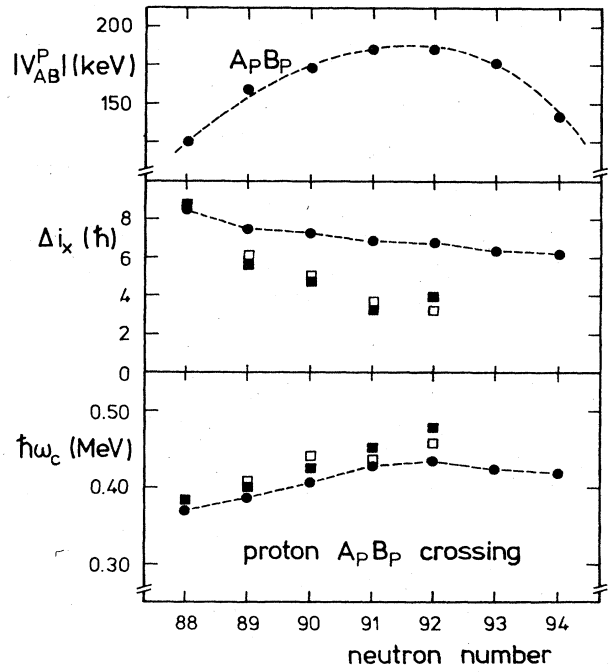

FIG. 16. Comparison between the experimental and calculated (CSM; see text) values of the crossing frequency ($\hbar\omega_c$) and alignment gain (Δi_x) for the A_pB_p proton crossing in the erbium isotopes $^{156-162}$Er. The calculated interaction strength (V^p_{AB}) is also shown. Solid circles correspond to the CSM values, and solid (yrast band) and open squares (negative parity sideband) to the experimental values.

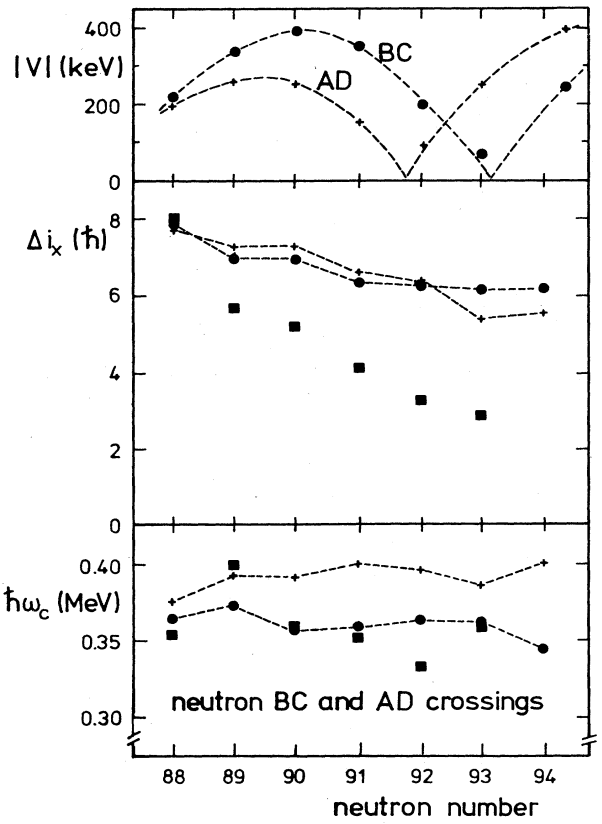

FIG. 17. Same as Fig. 16, but for the *BC* neutron crossing. The CSM values (crosses) for the *AD* neutron crossing are given as w[illegible].

and calculated crossing frequencies, but only a qualitative agreement for the alignment gains: experimentally, the latter decreases faster with the number of neutrons than predicted by the theory. Nevertheless, our ^{157}Er experimental data ($\hbar\omega_c = 0.40$ MeV, $\Delta i_x \geq 5.7\hbar$) fit better into the systematics of the A_pB_p proton crossing. Indeed, one expects a lower frequency for the *BC* neutron crossing ($\hbar\omega_c \cong 0.375$ MeV) than for the A_pB_p proton crossing ($\hbar\omega_c \cong 0.386$ MeV).

It has been stated by Riley *et al.*[20] that, in the favored band of ^{157}Er, the A_pB_p proton alignment coincides with the *BC* neutron alignment at a frequency of 0.40 MeV. In that case, however, the total gain of aligned angular momentum should be at least $10\hbar$: it is $8.7\hbar$ and $8.0\hbar$ for the A_pB_p and *BC* crossings, respectively, in ^{156}Er (Refs. 4 and 44), and $4.8\hbar$ and $5.2\hbar$ for the A_pB_p and *BC* crossings, respectively, in ^{158}Er, according to the experimental data of Riley *et al.*[20] This is not confirmed experimentally: even if the 803 keV transition claimed by these authors[20] exists somewhere in the favored band (see Sec. III A), $\Delta i_x \approx 7.7\hbar$; if not, $\Delta i_x \approx 5.7\hbar$. The critical frequency $\hbar\omega_c$ for the A_pB_p crossing increases experimentally with the neutron number in the Er isotopes (squares in Fig. 17). The suggestion of Riley *et al.*[20] that this trend is due to an increase of the quadrupole deformation between ^{157,158,159}Er (Fig. 2 of Ref. 20) is confirmed by the present CSM calculations (full points in Fig. 16), wherein the experimental deformations have been used (Table VII), which indeed show the proposed trend. However, the same CSM calculations, with the same deformations, predict (full points in Fig. 17) that the neutron *BC* crossing should happen in ^{157}Er at a definitely lower critical frequency ($\hbar\omega_c \cong 0.375$ MeV) than suggested by Riley *et al.*[20] ($\hbar\omega_c \cong 0.40$ MeV), in line with the experimental data on ^{156,158,159}Er (squares in Fig. 17). There are thus problems with the gain in aligned angular momentum and with the critical frequency if the A_pB_p and *BC* crossings are assumed to coincide in ^{157}Er.

It remains, however, that, from the point of view of our CSM calculations, the absence of the *BC* neutron crossing around $\hbar\omega = 0.375$ MeV in the favored band of ^{157}Er represents a problem. One possible explanation, which we have already discussed in Ref. 18, could be that the interaction $|V|$ at the *BC* crossing could be larger in this nucleus than in its neighbors, thereby making the crossing undiscernible. This would imply that the oscillations of $|V_{BC}|$ as a function of the neutron number would be shifted by one unit with respect to the present CSM calculations shown in Fig. 17. Nevertheless, we can safely conclude that, since the *BC* crossing is anyway blocked in the *s* band of even-even nuclei, only the A_pB_p proton crossing can be responsible for the second backbending observed in these nuclei, in particular in ^{158}Er.

From the data obtained in the present work, the nature of the sideband established in the nucleus ^{157}Er could not be determined. According to Riley *et al.*,[20] this band corresponds to the excited quasineutron configuration *EAB* below $\hbar\omega = 0.40$ MeV, and to the configuration *EAB* A_pB_p above $\hbar\omega = 0.40$ MeV.

C. Further information obtained from the experimental results

1. *Triaxial shape transition in ^{159}Tm*

One of the most striking features of the experimental data on the nucleus ^{159}Tm is the large signature splitting between the favored ($\alpha = -\frac{1}{2}$) and unfavored ($\alpha = +\frac{1}{2}$) bands at low spin, clearly visible in the $i_x(\omega)$ and $e'(\omega)$ plots of Fig. 13(c) [α is the band signature, which is connected with the total angular momentum I by $I = \alpha \bmod 2$ (Ref. 12)]. However, this splitting ($\Delta e' \cong 100$ keV at $\hbar\omega = 0.20$ MeV) almost completely disappears above the first backbending which is present in the two bands; a close examination of the data shows that the energy splitting is actually inverted above the band crossing ($\Delta e' \cong -15$ keV at $\hbar\omega = 0.40$ MeV). This particular behavior of the Routhians has also been observed in the isotone ^{157}Ho, as well as in the nuclei ^{155,159}Ho.[34]

According to a suggestion of Frauendorf and May,[46] this behavior could be explained by introducing a triaxial deformation for these nuclei, conveniently expressed by the parameter γ, where the Lund convention for the sign of γ has been used, and by assuming, furthermore, that the alignment of a neutron pair changes the value of γ. The CSM calculations we have carried out for ^{159}Tm with nonzero γ values show that the evolution of the signature splitting with rotational frequency can indeed be repro-

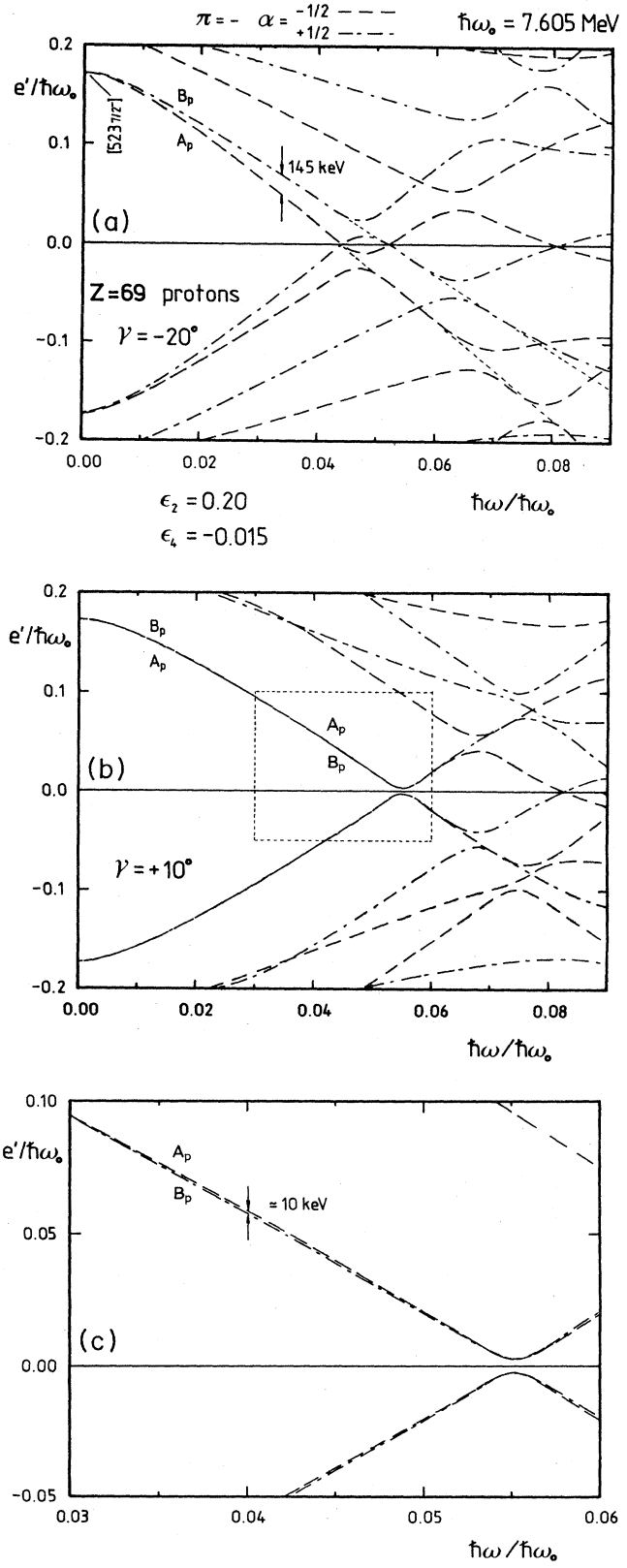

FIG. 18. Quasiparticle diagrams for protons in ^{159}Tm, calculated as outlined in Sec. IV B, with the parameters given in Table VII, and with $\gamma=-20°$ (a) and $\gamma=+10°$ (b). An enlarged part of (b) corresponding to the dotted rectangle is given in (c).

duced if one assumes that the deformation parameter γ changes from a negative value ($\gamma=-20°$) below the band crossing to a positive value ($\gamma=+10°$) above the band crossing (Fig. 18). In these calculations, the following (constant) parameters were used: $\epsilon_2=0.20$, $\epsilon_4=-0.015$, and $\Delta_p=0.171\hbar\omega_0$.

The triaxial shape transition observed in slightly deformed nuclei of the rare earth region can be understood, on a broad basis, by stating that the aligned nucleons "print" their orbital shape on the core.[47] These nuclei are accordingly called "γ soft."

2. *Magnetic dipole and electric quadrupole properties across the backbending in ^{159}Tm*

Figure 11 shows that the nucleus ^{159}Tm also displays a signature splitting for the values of $B(M1)/Q_0^2$, corresponding to the favored and unfavored branches of its yrast band. Furthermore, across the backbending region, this ratio experiences a steep rise, by a factor of 15 to 25.

Recent lifetime measurements[48] in the odd-Z nucleus ^{157}Ho, which behaves in a similar way as ^{159}Tm with respect to $B(M1)/Q_0^2$, have provided evidence that the electric quadrupole moment Q_0 only slightly decreases (by less than 10%) over the investigated frequency range, $\hbar\omega=0$–0.36 MeV. This means that the observed rise of $B(M1)/Q_0^2$ in ^{157}Ho is due to an important increase of the magnetic dipole matrix elements $B(M1)$ across the backbending region. According to the authors of Ref. 48, the observed slight decrease of Q_0 is consistent with a triaxial shape transition from a negative to a positive value, since Q_0 is proportional to $\cos(\gamma+30°)$.

In the nucleus ^{159}Tm, the change from $\gamma=-20°$ to $+10°$ across the backbending, suggested by the change of signature splitting as outlined in Sec. IV C *1*, would imply an associated 20% decrease of Q_0. Consequently, if one assumed that the electric quadrupole moment of ^{159}Tm experiences no stronger variation than that, Fig. 11 should essentially display the qualitative behavior of the reduced $M1$ transition probability. As $B(M1)$ is proportional to $(g_K-g_R)^2$ in the strong coupling limit, Fig. 11 would then suggest that g_K is very close to g_R before the backbending, and quite different above the backbending. This is consistent with a strong decrease of g_K, towards large negative values, associated with the alignment of a pair of $i_{13/2}$ neutrons at the first backbending in ^{159}Tm.

3. *Behavior of the moments of inertia at high rotational frequency*

Due to the Coriolis antipairing (CAP) effect,[49] the nuclear pairing correlations are expected to decrease, and possibly vanish, at very high rotational frequencies. Experimentally, information on these pairing correlations can be obtained by investigating the variation of the nuclear moment of inertia with the rotational frequency.[50] The kinematical and dynamical moments of inertia are defined by[27] $\mathcal{J}^{(1)}\equiv I_x/\omega$ and $\mathcal{J}^{(2)}\equiv dI_x/d\omega$, respectively. They can be calculated by taking for I_x, either the collective rotation contribution only, or the collective rotation *and* particle alignment contributions,[51] in which cases the

moments of inertia are called collective ($\mathcal{I}_{\rm coll}$) or effective ($\mathcal{I}_{\rm eff}$), respectively. The quantities $\mathcal{I}^{(1)}_{\rm eff}$ and $\mathcal{I}^{(2)}_{\rm eff}$ can be deduced from the discrete transition energies in one band. The value of $\mathcal{I}^{(2)}_{\rm coll}$ is generally determined from transition energy correlation measurements.[22] In fact, the width W of the central valley, which can usually be observed in a continuum-subtracted $E_{\gamma 1}\times E_{\gamma 2}$ matrix, is inversely proportional to $\mathcal{I}^{(2)}_{\rm coll}$,

$$\mathcal{I}^{(2)}_{\rm coll}=\frac{8\hbar}{W}\ .$$

A contour plot of the $\geq$ onefold $E_{\gamma 1}\times E_{\gamma 2}$ coincidence matrix we have recorded for the ^{141}Pr + ^{22}Ne(120 MeV) reaction, after subtraction of the uncorrelated events, is shown in Fig. 19, and spectra corresponding to cuts perpendicular to the main diagonal are displayed in Fig. 20. It is apparent that the width of the central valley decreases with increasing rotational frequency, and hence that the collective moment of inertia $\mathcal{I}^{(2)}_{\rm coll}$ increases with $\hbar\omega$. It is, however, difficult to extract accurate values of $\mathcal{I}^{(2)}_{\rm coll}$ from these data, due to the limited statistics available, to the uncertainties in the uncorrelated background substraction procedure (Sec. II A *2*), and to the lack of sharp "ridges" delimiting the central valley (Figs. 19 and 20). Consequently, the plot of $\mathcal{I}^{(2)}_{\rm coll}$ vs $\hbar\omega$ shown in Fig. 21 should only give the general trend of the variation of the former as a function of the latter. It should also be noticed that, although the (^{22}Ne,4n) reaction leading to ^{159}Tm dominates in the plot of Fig. 19 (Sec. III B), other neighboring nuclei also contribute to this diagram.

In Fig. 21, the values of $\mathcal{I}^{(1)}_{\rm eff}$ and $\mathcal{I}^{(2)}_{\rm eff}$ vs $\hbar\omega$ for the $\pi h_{11/2}$ band in ^{159}Tm are also shown; $\mathcal{I}^{(2)}_{\rm eff}$ is only displayed for $\hbar\omega>0.3$ MeV, since this quantity experiences wild variations in the backbending region, outside the scale of Fig. 21, as is well known.[50] The rigid moment of inertia $\mathcal{I}_{\rm rigid}$ has been computed for an ellipsoidally shaped rigid body with $A=159$ and $\epsilon_2=0.20$, yielding a value of 68.5 MeV$^{-1}\hbar^2$, also indicated in Fig. 21.

In spite of the above-mentioned words of caution, the data displayed in Fig. 21 suggest that, with increasing rotational frequency, $\mathcal{I}^{(1)}_{\rm eff}$, $\mathcal{I}^{(2)}_{\rm eff}$, and $\mathcal{I}^{(2)}_{\rm coll}$ tend towards the same constant value, which is close to the calculated $\mathcal{I}_{\rm rigid}$. This could be interpreted[50] as an indication that the pairing correlations are strongly reduced at rotational frequencies above $\hbar\omega=0.50$ MeV in ^{159}Tm. Similar features have recently been observed in some other deformed nuclei, i.e., ^{84}Zr,[52] ^{130}Ce,[53] and ^{168}Hf,[54] and similar conclusions have been drawn in these cases. It should, however, be pointed out that the relation between the above-mentioned behavior of the various moments of inertia and the evidences for pairing collapse has recently been questioned,[55] so that further work on this problem, experimental and theoretical, is clearly needed.

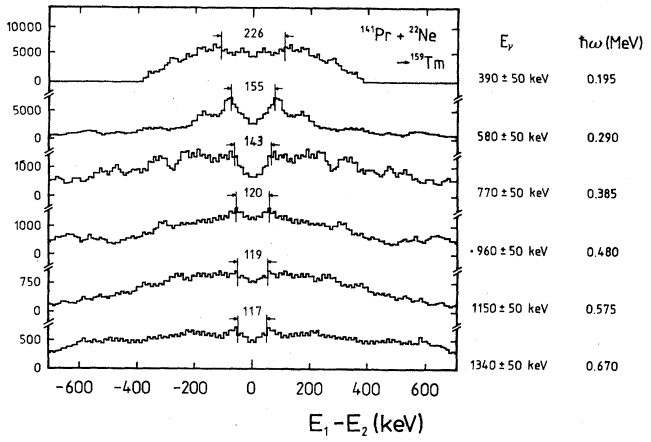

FIG. 20. Cuts perpendicular to the main diagonal in the $E_{\gamma 1}\times E_{\gamma 2}$ contour plot of Fig. 19. The corresponding values of $E_\gamma=(E_{\gamma 1}+E_{\gamma 2})/2$ are given on the right-hand side, together with the associated rotational frequencies $\hbar\omega$. The width of the central valley, in keV, is indicated for each cut.

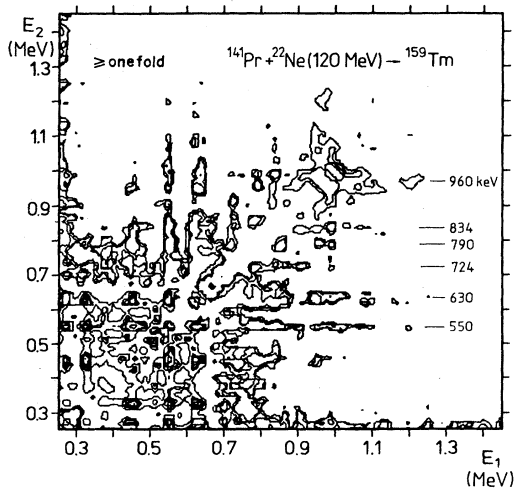

FIG. 19. Transition energy correlations, i.e., $E_{\gamma 1}\times E_{\gamma 2}$ contour plot, for the ^{141}Pr(^{22}Ne,5n)^{159}Tm reaction at $E(^{22}\text{Ne})=120$ MeV. Prominent transitions in ^{159}Tm (Table II) are indicated by thin horizontal lines, with their energies in keV. The energy scales on the E_1 and E_2 axes are given in MeV.

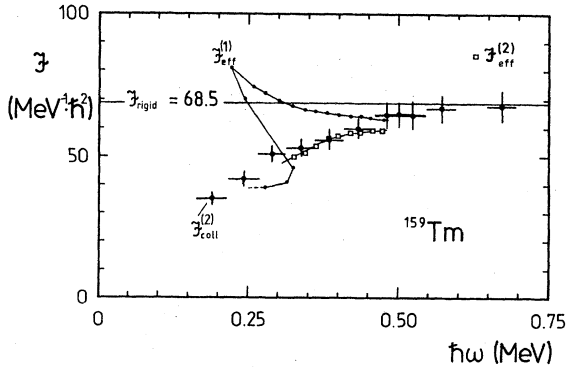

FIG. 21. Plot of the effective and collective moments of inertia, $\mathcal{I}^{(1)}_{\rm eff}$, $\mathcal{I}^{(2)}_{\rm eff}$, and $\mathcal{I}^{(2)}_{\rm coll}$, defined and deduced as outlined in Sec. IV C *3* vs the rotational frequency $\hbar\omega$, for the nucleus ^{159}Tm. The calculated value of the rigid moment of inertia $\mathcal{I}_{\rm rigid}$ is also indicated.

V. SUMMARY

In the present work, high-spin states have been investigated in the odd-N nucleus ^{157}Er and in the odd-Z nucleus ^{159}Tm by the ^{122}Sn(^{40}Ar,5n) and ^{141}Pr(^{22}Ne,4n) reactions, respectively. In ^{157}Er, the favored band ($\alpha=+\frac{1}{2}$) has been established up to the $I^{\pi}=\frac{53}{2}^{+}$ level, corresponding to a rotational frequency $\hbar\omega=0.417$ MeV; in ^{159}Tm, the favored ($\alpha=-\frac{1}{2}$) and unfavored ($\alpha=+\frac{1}{2}$) bands have been measured up to the levels with $I^{\pi}=\frac{59}{2}^{-}$ ($\hbar\omega=0.454$ MeV) and $\frac{61}{2}^{-}$ ($\hbar\omega=0.480$ MeV), respectively. In the two nuclei, this is well above the frequency region where a second backbending is known to occur in the neighboring even-even nuclei. A sharp upbending has been observed in the favored band of ^{157}Er at $\hbar\omega=0.40$ MeV, whereas in ^{159}Tm, no evidence for a pair alignment in the frequency range 0.30 MeV $\lesssim\hbar\omega\lesssim$0.48 MeV has been obtained. Data have also been obtained on a sideband in ^{157}Er, as well as on the $(\nu i_{13/2})$ $(\pi h_{11/2})$ bands in the odd-odd nucleus ^{158}Tm.

The experimental data have been interpreted in the framework of the cranked shell model. The comparison of the experimental crossing frequencies and gains in aligned angular momentum with CSM calculations on the one hand, and with the experimental systematics of neighboring nuclei on the other hand, shows that the upbending in ^{157}Er is connected with the A_pB_p proton crossing, which is blocked in the two branches of the $h_{11/2}$ yrast band of ^{159}Tm. One can thereby conclude that the second backbending observed in the yrast band of even-even nuclei near $A=158$ is due to the RAL of a pair of $h_{11/2}$ protons.

Furthermore, in the present work, evidence has been obtained for a triaxial shape transition in the nucleus ^{159}Tm. Indeed, the reduction, and even inversion, of the energy splitting between the Routhians with signatures $\alpha=+\frac{1}{2}$ and $-\frac{1}{2}$ above the first backbending can only be explained, in the framework of CSM calculations, by assuming a change from a negative to a positive value for the triaxiality parameter γ.

The analysis of the discrete transition energies and of the transition energy correlations in the nucleus ^{159}Tm has yielded information on the evolution of the kinematical and dynamical moments of inertia at extremely high rotational frequencies. These results suggest that, above $\hbar\omega\cong0.50$ MeV, $\mathcal{I}^{(1)}_{\text{eff}}$, $\mathcal{I}^{(2)}_{\text{eff}}$, and $\mathcal{I}^{(2)}_{\text{coll}}$ approach the rigid rotor value. The possible implications of this remark on the expected transition from the superfluid to the normal phase (pairing collapse) have been discussed.

ACKNOWLEDGMENTS

The authors wish to thank Dr. Y. Jongen, Dr. G. Ryckewaert, and Dr. C. Pirart for the efficient running of the Cyclone accelerator facility, Prof. J. Kuzminski for his assistance in the early stages of this work, Mr. P. Demaret for his skillful technical help during the course of the experiments, and Mr. H. Folger, from the Gesellschaft für Schwerionenforschung (GSI), Darmstadt, for the preparation of the thin targets used in this experiment.

[1] I. Y. Lee, M. M. Aleonard, M. A. Deleplanque, Y. El Masri, J. O. Newton, R. S. Simon, R. M. Diamond, and F. S. Stephens, Phys. Rev. Lett. **38**, 1454 (1977).

[2] F. A. Beck, E. Bozek, T. Byrski, C. Gehringer, J. C. Merdinger, Y. Schutz, J. Styczen, and J. P. Vivien, Phys. Rev. Lett. **42**, 493 (1979).

[3] L. L. Riedinger, O. Andersen, S. Frauendorf, J. D. Garrett, J. J. Gaardhøje, G. B. Hagemann, B. Herskind, Y. V. Makovetzky, J. C. Waddington, M. Guttormsen, and P. O. Tjøm, Phys. Rev. Lett. **44**, 568 (1980).

[4] T. Byrski, F. A. Beck, C. Gehringer, J. C. Merdinger, Y. Schutz, and J. P. Vivien, Phys. Lett. **102B**, 235 (1981).

[5] L. L. Riedinger, S. Frauendorf, H. Ower, and L. H. Courtney, in *Proceedings of the International Conference on High Angular Momentum Properties of Nuclei, Oak Ridge, 1982,* edited by N. R. Johnson (Harwood, New York, 1982), Vol. 1, p. 8.

[6] A. Faessler and M. Ploszajczak, Phys. Lett **76B**, 1 (1978).

[7] R. M. Lieder and H. Ryde, in *Advances in Nuclear Physics,* edited by M. Baranger and E. Vogt (Plenum, New York, 1978), Vol. 10, p. 1.

[8] F. S. Stephens and R. S. Simon, Nucl. Phys. **A183**, 257 (1972).

[9] E. Grosse, F. S. Stephens, and R. M. Diamond, Phys. Rev. Lett. **31**, 840 (1973).

[10] E. Grosse, F. S. Stephens, and R. M. Diamond, Phys. Rev. Lett. **32**, 74 (1974).

[11] M. Ploszajczak and A. Faessler, Nucl. Phys. **A379**, 77 (1982).

[12] R. Bengtsson and S. Frauendorf, Nucl. Phys. **A327**, 139 (1979).

[13] J. Dudek, W. Nazarewicz, and Z. Szymański, Phys. Scr. **24**, 309 (1981).

[14] H. Beuscher, W. F. Davidson, R. M. Lieder, and A. Neskakis, Nucl. Phys. **A249**, 379 (1975).

[15] A. J. Larabee and J. C. Waddington, Phys. Rev. C **24**, 2367 (1981).

[16] R. Bengtsson and S. Frauendorf, Nucl. Phys. **A314**, 27 (1979).

[17] R. Holzmann, J. Kuzminski, M. Loiselet, M. A. Van Hove, and J. Vervier, in *Proceedings of the International Conference on High Angular Momentum Properties of Nuclei, Oak Ridge, 1982,* edited by N. R. Johnson (Harwood, New York, 1982), Vol. 1, p. 2; Verh. Dtsch. Phys. Ges. **5**, 1140 (1983).

[18] R. Holzmann, J. Kuzminski, M. Loiselet, M. A. Van Hove, and J. Vervier, Phys. Rev. Lett. **50**, 1834 (1983).

[19] L. L. Riedinger, L. H. Courtney, A. J. Larabee, J. C. Waddington, M. P. Fewell, N. R. Johnson, I. Y. Lee, and F. K. McGowan, in *Proceedings of the International Conference on High Angular Momentum Properties of Nuclei, Oak Ridge, 1982,* edited by N. R. Johnson (Harwood, New York, 1982), Vol. 1, p. 4.

[20] M. A. Riley, J. Simpson, R. Aryaeinejad, J. R. Cresswell, P. D. Forsyth, D. Howe, P. J. Nolan, B. M. Nyakó, J. F. Sharpey-Schafer, P. J. Twin, J. Bacelar, J. D. Garrett, G. B. Hagemann, B. Herskind, and A. Holm, Phys. Lett. **135B**, 275 (1984).

[21] Y. Jongen, C. Pirart, and G. Ryckewaert, in *Proceedings of the Ninth International Conference on Cyclotrons and Their Applications,* edited by G. Gendreau (Editions de Physique,

Paris, 1981), p. 281.
[22]O. Andersen, J. D. Garrett, G. B. Hagemann, B. Herskind, D. L. Hillis, and L. L. Riedinger, Phys. Rev. Lett. **43**, 687 (1979).
[23]B. Herskind, J. Phys. C **10**, 106 (1980).
[24]R. Bauer, Phys. Rev. C **19**, 399 (1979).
[25]S. Y. Van der Werf, Nucl. Instrum. Methods **153**, 221 (1978).
[26]M. A. Deleplanque, T. Byrski, R. M. Diamond, H. Hübel, F. S. Stephens, B. Herskind, and R. Bauer, Phys. Rev. Lett. **41**, 1105 (1978).
[27]A. Bohr and B. R. Mottelson, Phys. Scr. **24**, 71 (1981).
[28]F. S. Stephens, J. Phys. C **10**, 1 (1980).
[29]W. Ockels, Z. Phys. A **286**, 181 (1978).
[30]D. L. Hillis, J. D. Garrett, O. Christensen, B. Fernandez, G. B. Hagemann, B. Herskind, B. B. Back, and F. Folkmann, Nucl. Phys. **A325**, 216 (1979).
[31]*Table of Isotopes,* 7th ed., edited by C. M. Lederer and V. S. Shirley (Wiley, New York, 1978).
[32]J. Burde, E. L. Dines, S. Shih, R. M. Diamond, J. E. Draper, K. H. Lindenberger, C. Schück, and F. S. Stephens, Phys. Rev. Lett. **48**, 530 (1982).
[33]I. Adam, M. Honusek, Z. Hons, V. V. Kuznetsov, T. M. Muminov, R. R. Usmanov, and A. Budziak, Nucl. Phys. **A356**, 129 (1981).
[34]G. B. Hagemann, J. D. Garrett, B. Herskind, G. Sletten, P. O. Tjøm, A. Henriques, F. Ingenbretsen, J. Rekstad, G. Løvhøiden, and T. F. Thorsteinsen, Phys. Rev. C **25**, 3224 (1982).
[35]S. Drissi, S. André, J. Genevey, V. Barci, A. Gizon, J. Gizon, J. A. Pinston, J. Jastrzebski, R. Kossakowski, and Z. Preibisz, Z. Phys. A **302**, 361 (1981).
[36]R. Bengtsson, S. Frauendorf, and F. R. May, At. Data Nucl. Data Tables (to be published).
[37]S. M. Harris, Phys. Rev. **138**, B509 (1965).
[38]A. H. Wapstra and K. Bos, At. Data Nucl. Data Tables **19**, 175 (1977).
[39]A. Bohr and B. R. Mottelson, *Nuclear Structure* (Benjamin, New York, 1969), Vol. 1, p. 170.
[40]S. Frauendorf, in *Proceedings of the Nuclear Physics Workshop, Trieste, 1981,* edited by C. H. Dasso, R. A. Broglia, and A. Winther (North-Holland, Amsterdam, 1982), p. 111.
[41]W. Andrejtscheff, K. D. Schilling, and P. Manfrass, At. Data Nucl. Data Tables **16**, 515 (1975).
[42]K. E. G. Löbner, M. Vetter, and V. Hönig, Nucl. Data Tables **A7**, 495 (1970).
[43]R. Bengtsson, J. Phys. C **10**, 84 (1980).
[44]A. W. Sunyar, E. Der Mateosian, O. C. Kistner, A. Johnson, A. H. Lumpkin, and P. Thieberger, Phys. Lett. **62B**, 283 (1976).
[45]J. D. Garrett, G. B. Hagemann, B. Herskind, J. Bacelar, R. Chapman, J. C. Lisle, J. N. Mo, A. Simcock, J. C. Willmott, and H. G. Price, Phys. Lett. **118B**, 297 (1982).
[46]S. Frauendorf and F. R. May, Phys. Lett. **125B**, 245 (1983).
[47]G. A. Leander, S. Frauendorf, and F. R. May, in *High Angular Momentum Properties of Nuclei, Oak Ridge, 1982,* edited by N. R. Johnson (Harwood, New York, 1982), p. 281.
[48]G. B. Hagemann, J. D. Garrett, B. Herskind, J. Kownaki, B. M. Nyakó, P. J. Nolan, J. F. Sharpey-Schafer, and P. O. Tjøm, Nucl. Phys. **A424**, 365 (1984).
[49]A. Faessler, W. Greiner, and R. K. Sheline, Nucl. Phys. **62**, 241 (1965).
[50]M. J. A. de Voigt, J. Dudek, and Z. Szymański, Rev. Mod. Phys. **55**, 949 (1983).
[51]R. M. Diamond and F. S. Stephens, Annu. Rev. Nucl. Part. Sci. **20**, 85 (1980).
[52]H. G. Price, C. J. Lister, B. J. Varley, W. Gelletly, and J. W. Olness, Phys. Rev. Lett. **51**, 1842 (1983).
[53]P. J. Nolan, R. Aryaeinejad, A. H. Nelson, D. J. G. Love, D. M. Todd, and P. J. Twin, Phys. Lett. **128B**, 285 (1983).
[54]R. Chapman, J. C. Lisle, J. N. Mo. E. Paul, A. Simcock, J. C. Willmott, J. R. Leslie, H. G. Price, P. M. Walker, J. C. Bacelar, J. D. Garrett, G. V. Hagemann, B. Herskind, A. Holm, and P. J. Nolan, Phys. Rev. Lett. **51**, 2265 (1983).
[55]B. Herskind, in *Proceedings of the International Conference on Nuclear Physics, Florence, 1983,* edited by P. Blasi and R. A. Ricci (Tipografia Compositori, Bologna, 1983), Vol. 2, p. 117.